MODELING AND VALIDATING A CONTINUOUS FLOW ULTRAVIOLET LIGHT EMITTING DIODE WATER PURIFICATION REACTOR

THESIS

David A. Kohlhepp, Capt, USAF

AFIT-ENV-MS-17-M-198

DEPARTMENT OF THE AIR FORCE
AIR UNIVERSITY

AIR FORCE INSTITUTE OF TECHNOLOGY

Wright-Patterson Air Force Base, Ohio

AFIT-ENV-MS-17-M-198

MODELING AND VALIDATING A CONTINUOUS FLOW ULTRAVIOLET LIGHT EMITTING DIODE WATER PURIFICATION REACTOR

THESIS

Presented to the Faculty

Department of Engineering and Management

Graduate School of Engineering and Management

Air Force Institute of Technology

Air University

Air Education and Training Command

In Partial Fulfillment of the Requirements for the

Degree of Master of Science in Engineering Management

David A. Kohlhepp, BS

Captain, USAF

March 2017

AFIT-ENV-MS-17-M-198

MODELING AND VALIDATING A CONTINUOUS FLOW ULTRAVIOLET LIGHT EMITTING DIODE WATER PURIFICATION REACTOR

David A. Kohlhepp, BS
Captain, USAF

Committee Membership:

Dr. Michael E. Miller, PhD
Chair

Dr. Willie F. Harper Jr., PhD, P.E.
Member

Dr. Diedrich Prigge V, PhD
Member

Abstract

The Department of Defense has a need for a small, man-portable, point of use water purification device that is not currently available commercially in a configuration that meets all the use requirements. A device that utilizes ultraviolet (UV) light-emitting diodes (LEDs) to continuously treat water flowing from a "dirty" reservoir to a "clean" reservoir with low weight and power penalties would meet those requirements. This research pursued the development of such a device through the use of computer modeling, specifically in the area of computational fluid dynamics (CFD) and transport of diluted species. It sought to validate the use of the model for design optimization by duplicating concentration tracer tests accomplished in a laboratory with a prototype UV LED reactor at four different flow rates. By measuring the tracer concentration over time at the reactor effluent, the model results were compared to the experimental data qualitatively by the residence time density functions and quantitatively by hydraulic residence times, density curve characteristics, and the dispersion coefficient. The research found that the model has difficulty accurately reproducing the experimental results at lower flow rates, but finds success at the higher rates, rendering the model a useful tool for prototype design and development.

Acknowledgments

I would like to express my sincere appreciation to my faculty advisor for his guidance and support throughout the course of this thesis effort. The insight and experience was certainly appreciated. I would also like to thank my wife for her unending support and encouragement on our journey together.

David A. Kohlhepp

Table of Contents

List of Figures

List of Tables

MODELING AND VALIDATING A CONTINUOUS FLOW ULTRAVIOLET LIGHT EMITTING DIODE WATER PURIFICATION REACTOR

I. Introduction

General Issue

The US Military is engaged in operations across the globe in significantly different environments, each with significantly different requirements. It is neither feasible nor practical for the military to develop in-house solutions for all the logistical and technological requirements those operations produce. As such, the military frequently turns to commercial off-the-shelf (COTS) products to supplement or augment its own gear and equipment. In fact, according to a report by the Defense Science Board Task Force on Integrating Commercial Systems into the DOD, Effectively and Efficiently, utilization of COTS products can produce lower costs, quicker implementation, lower risk, and proven performance (Schneider Jr., 2009). Additionally, the Federal Acquisition Regulation (FAR) Subpart 12.103 - Commercially Available Off-the-Shelf (COTS) Items provides the framework and process for acquiring COTS products for government use (*Federal Acquisition Regulation*, 2016).

In the field of water purification, the military utilizes equipment like the Reverse Osmosis Water Purification Unit (ROWPU) to produce clean water for consumption. It is a large-scale piece of kit, capable of producing 1,500 gallons of water per hour using, 35 kilowatts of power (AFH 10-222, Vol 9 2011). However, it is cumbersome to transport and not at all practical for small team or individual use. A small, man-portable, point of use system could meet clean water needs in situations where pieces of equipment like the ROWPU are impractical. Specifically, a small “fire and forget” device that

utilizes ultraviolet (UV) light-emitting diodes (LEDs) to continuously treat water flowing from a "dirty" reservoir through a particulate pre-filter to a "clean" reservoir with low weight and power penalties would meet that need. Such equipment could be used by small teams in remote locations with limited logistical support or even as part of an aircrew survival kit.

Traditionally, this technology would be an excellent candidate for a COTS procurement. Numerous devices that use a wide range of methods of filtering or reducing the viability of microorganisms in water are available, as is evident in the civilian outdoor recreation market. Design goals shared among them are light weight, durability, portability, and efficiency. These are the same objectives the U.S. Air Force has for a water purification unit. However, none of them currently combine all those design features while still meeting the military's intended use and criteria, so a COTS solution would not be viable for these objectives. As such, this research seeks to advance the field of continuous flow UV LED water purification for military application.

Research in this area has been underway at the Air Force Institute of Technology since 2013 (Spencer, 2014). Since then, researchers have created and tested a number of prototypes using a variety of materials and configurations in attempts to find a geometry that provides the most efficient treatment possible. Each researcher has designed and built a reactor, then evaluated the reactor's efficiency by conducting an advanced oxidation process (AOP) with different dyes or microorganism inactivation experiments using virus spores or bacteria. Each set of evaluations led to new discoveries that informed the next prototype design. The reactors shrunk in size and evolved from stainless steel to Polytetrafluoroethylene (PTFE) construction. This process is inefficient,

however, due to the long lead times and financial costs associated with physically constructing and testing each iteration of the reactor and the difficulties associated with altering more than one variable at a time. The next logical step would be to conduct the initial design and testing digitally by building a computer-based model of the reactor and evaluating it with a physics-based software system. Beginning in 2015, Drew Gallucci utilized the COMSOL Multiphysics® Modeling Software to create a simple model of the fluid flow in his reactor prototype (2016). COMSOL Multiphysics® is a general-purpose software platform, based on advanced numerical methods, for modeling and simulating physics-based problems that can account for coupled or Multiphysics phenomena (COMSOL, 2016). In this application, COMSOL Multiphysics® would be able to simulate and model the physical interaction between the fluid flow, ray optics, and transport of diluted species. Using COMSOL, researchers would be able to design, build, and test their reactors digitally before investing the significant time and monetary resources to construct a physical model. Further, these models would provide insight into the processes occurring in the reactor, providing information on potentially fruitful design perturbations. Once their design was optimized, they would be able to build and test the physical model to validate the digital results.

Due to the complexities of such an intricate model, a logical first step would be to model and test the physics independently, or in pairs, before implementing all aspects at once. Those results could be validated in the laboratory with one of the existing reactor prototypes. If the laboratory results match the model results, the modeling effort can continue until the goal of an optimized, validated, and fully functioning reactor model is attained.

Problem Statement

The US Military excels at producing large quantities of pure water from a wide variety of sources, but its flexibility is limited in austere environments with small-scale demands. COTS products may meet some requirements, but are not optimized for this particular use. As such, the military has application for a small, man-portable, point of use water purification device. When utilized in a continuous flow, backpack-type system, UV LEDs have the potential to meet the military's objectives while still maintaining a light weight and low energy demand. Although multiple iterations of prototypes have been developed, the optimized configuration of physical geometry, material type, and number and orientation of the LEDs has not yet been identified. Additionally, the COMSOL Multiphysics® modeling software has not been validated with the existing prototype reactors in this application.

Research Objective

The objective of this research is to implement the powerful capabilities of a modeling software like COMSOL Multiphysics® to digitize the prototype process. This research represents a first step towards a fully functioning and validated model.

Research Focus

The focus of this thesis is to establish a baseline model of the fluid flow and transport of diluted species elements of the reactor and validate its application through laboratory testing of an existing reactor prototype.

Investigative Questions

This thesis investigates the following questions:

1) Can a model be created that accurately predicts the interaction between fluid flow and transport of diluted species?

2) Can that model account for the variance in behavior which results from varying flow rates?

3) Can the model be validated using real-world laboratory results?

Methodology

The methodology used in this thesis is modeling and experimentation. The first aspect was to develop and execute the laboratory experimentation to produce the observed data with which the model results were validated. The reactor was operated at 1 mL/min, 2 mL/min, 4 mL/min, and 8 mL/min. A slug of dye was inserted into the reactor, and the effluent concentration was measured at one-tenth of a second intervals for the 2 mL/min, 4 mL/min, and 8 mL/min flow rates and two-tenths of a minute (min) for the 1 mL/min flow rate until no more dye remained in the reactor.

COMSOL Multiphysics® was used to develop a computer-based model of the reactor. The physical geometry of the reactor was constructed within the program, and the fluid flow and transport of diluted species physics elements were implemented. The model operated at the same flow rates as the experimentation, and the concentration output was produced. The researcher was then able to compare the concentration curves and residence times to validate the model.

Assumptions/Limitations

Only one iteration of each flow rate and stir condition was completed for the laboratory testing phase. Both the laboratory and reactor prototype were in use by multiple researchers with similar methodology, so access and time were limited. However, anomalies related to methodology or the results are unlikely as the experimentation procedure was well-understood, and the results were within expected values. Therefore, it is assumed that these runs are indicative of reactor performance. Another limitation was the dye application flow rate. The dye was injected into the reactor via syringe by hand, so there may have been some slight variations in flow rate.

II. Literature Review

History of UV Drinking Water Disinfection

UV Germicidal Irradiation (UVGI) is the industry standard term (developed by the International Commission on Illumination) that refers to the use of UV light for disinfection, specifically using wavelengths in the germicidal range, or 200-320 nm (Kowalski, 2009). The UVGI term typically refers to surface and air disinfection, but some publications use it more broadly to include water purification. UV wavelengths are also referred to by band. The "C" band, or UVC, is considered germicidal and covers 200-280 nm, and the "B" band, or UVB, also germicidal, covers 280-320 nm. UVA, 320-400 nm, is not considered germicidal (Kowalski, 2009).

Arthur Downes and Thomas P. Blunt recorded the first known use of UV light as a germicide in a paper published by the Royal Society of London in 1878 (Downes & Blunt, 1878). They discovered that UV light is "inimical to" and under the right conditions may "wholly prevent" the growth of bacteria and other microorganisms. Downes and Blunt further developed their research by proving that the light's ability to prevent the growth of bacteria depended on the intensity, duration, and wavelength of the light (Reed, 2010). In 1903, Niels Ryberg Finsen was awarded the Nobel Prize for Medicine for his work in 1895 using UV light to treat a form of tuberculosis known as lupus vulgaris (Nobelprize.org, 2014). As tuberculosis is a bacterial disease, Finsen had some success treating it with concentrated UV light. As such, light therapy became a popular method of treating similar diseases until antibiotics rose to prominence. While the first use of UV to treat drinking water was in 1906 (Kowalski, 2009), the first record

of a commercial UV light treatment facility for drinking water was in Marseilles, France in 1910 (S. Clarke, 2006). Although novel, the plant suffered from technical faults, unreliable lamps, and power supply stability issues. Therefore, the plant was shut down shortly after initiation (James R. Bolton & Cotton, 2008). The first use of UV disinfection for drinking water in the US was in Henderson, KY in 1916 (Kowalski, 2009). By the 1920s, the use of chlorine for commercial drinking water was introduced and became popular due to its lower cost and ease of use. Subsequently, the use of UV disinfection was not reinvigorated until the 1950s (James R. Bolton & Cotton, 2008). In 1955, specifically, Switzerland and Austria installed the first modern drinking water UV disinfection systems using low-pressure UV lamps, and by 1985 there were over 1,500 similar plants across Europe (James R. Bolton & Cotton, 2008). The US lagged Europe in widespread implementation due to the perception that UV treatment was not effective against protozoa. It was not until 1998 that Bolton et al. (J.R. Bolton, Dussert, Bukhari, Hargy, & Clancy, 1998) found that UV light was indeed effective against chlorine-resistant Cryptosporidium and Giardia that there was a renewed interest in UV disinfection of drinking water in the US. That discovery, along with the earlier discovery of disinfection byproducts from the chlorine process that UV processes do not produce, led to a resurgence of UV treatment facilities (James R. Bolton & Cotton, 2008).

UV Lamp Development

Charles Wheatstone invented the mercury arc vapor lamp in 1835 that produced UV lines on the spectrum, but it proved to be unstable (Kowalski, 2009). It was not until 1896 that Herbert Dowsing and Henry Keating of London patented the first mercury

vapor lamp that was commercially viable (Perkin, 1910). Further development of mercury-based lights occurred in 1901, and then the benefits of quartz as a UV light transmitting material were realized in 1906 (Pirnie, Linden, & Malley, 2006). In the 1930s, the fluorescent lamp was introduced which led to germicidal tubular lamps (Pirnie et al., 2006). Mercury-based lamps produce UV light with a wavelength of 253.7, which is in the ideal germicidal range (Meulemans, 1987). Therefore, most UV lamps used for UVGI use a gas mixture that contains mercury, although xenon can be used as well (Pirnie et al., 2006). In addition to large-scale applications, UV tube lamps have recently been applied to small-scale, POU applications for residential or developing nation uses (Chatterley & Linden, 2010).

Although traditional UV lamps are effective in germicidal applications, there is a significant disadvantage associated with their use. Most UV lamps used for disinfection use between 5 and 400mg of mercury (S. Clarke, 2006). Mercury is toxic, and can be released as a vapor into the atmosphere or water supply if the lamps break (Chatterley & Linden, 2010). Although the concentration in the water due to a breakage may not be high, it would still be a health risk. There are other disadvantages of traditional UV sources as well that include lifetime, transportation, disposal, power requirements, monochromatic output, ballast cooling, sleeve fogging, and size/design limitations.

The emerging technology of UV LEDs addresses many of these disadvantages. LEDs are semiconductor devices that traditionally have emitted infrared or visible light when electric currents pass through them ("LED," 2016). They are created by connecting n-type and p-type layers of semiconductors. When the device is exposed to proper electric field, electrons flow from the n-type semiconductor and combine with holes in

the p-type semiconductor, near the interface. As the molecules in a proper p-type semiconductor undergo relaxation, the energy is released as photons as the electron drops into a lower orbital within the atom and light is created. The wavelength of the light is determined by the type of materials of the semiconductors (Bowker, Sain, Shatalov, & Ducoste, 2011) as the energy level of the photon depends upon the energy level between the atomic orbitals. Although there were some discoveries previously, the first breakthrough in LED technology was in 1962 at General Electric when Nick Holonyak Jr. developed the first visible-spectrum LED that emitted red light (Holonyak & Bevacqua, 1962). Approximately ten years later, orange, yellow, and green colored LEDs were developed by M. George Craford (Kovac, Peternai, & Lengyel, 2003). Finally, blue color-producing LEDs were not developed until 1993 (Nakamura, Mukai, & Senoh, 1994). The breakthrough for UV LEDs occurred around the same time as blue LEDs (Schubert, 2006), but it was not until 2000 that commercial UV LEDs became viable (Muramoto, Kimura, & Nouda, 2015). Currently, both UV and visible light LED technology is still advancing. Lenk and Lenk (2011) describe Haitz's Law, developed by Ronald Haitz and colleagues in 2006, which predicts that the luminous output of LED devices increases at a rate of 35% per year while the cost per lumen decreases at 20% per year. They go on to claim that the $100 billion lighting industry is currently undergoing a revolution. LED-based lighting is replacing other traditional light incandescent and fluorescent light sources, and it will soon become the lighting standard. (Lenk & Lenk, 2011).

UV LED Disinfection Advantages

The use of UV LEDs provides many advantages to the use of mercury lamps in drinking water disinfection. The first is that mercury lamps only emit at one wavelength, 253.7, whereas LEDs can be built to emit at specific wavelengths, covering a larger section of the germicidal wavelength range (Shur & Gaska, 2008). LED wavelength can be fine-tuned to achieve maximum disinfection efficiency by adjusting the semiconductor materials (Bowker et al., 2011).

Another advantage is that UV LEDs have no toxic elements. There is no risk of atmospheric or water pollution in the event of a broken bulb. In fact, the long term viability of existing UV florescent bulbs is in question as the United Nations Environment Program (UNEP) signed an agreement to limit mercury use and mining by 2020, impacting products that use mercury (Jenny, Jasper, Simmons, Shatalov, & Ducoste, 2015). Additionally, the lack of mercury along with glass or filament makes disposal much simpler (Chatterley & Linden, 2010).

The next advantage is the lack of warm-up time needed for UV LEDs. Mercury tubes can take up to 400 seconds to reach full output (Crawford et al., 2005). LEDs can be activated instantaneously, eliminating warm-up time, saving energy, and allowing for intermittent use (Chatterley & Linden, 2010).

One disadvantage of mercury lamps is their size and shape. They're typically long tubes, which can limit design considerations, making them impractical for POU systems (Jenny et al., 2015). UV LEDs' small size make them modular and increase the number of practical system configurations.

Finally, UV LEDs provide other advantages including lower costs from energy savings, fewer maintenance requirements, longer replacement intervals (Chatterley & Linden, 2010), lower voltages, a reduction in auxiliary electronics, and lower overall cost when compared to similar mercury systems (Crawford et al., 2005). All these factors, combine with UV LEDs' Haitz's Law growth and development rate, make UV LEDs a compelling alternative or even means for future drinking water UV disinfection systems.

Current Water Treatment Methods

One of the most basic methods for treating water is boiling. Boiling water can kill all micro-organisms that cause disease. The Centers for Disease Control (CDC) advises heating water to a rolling boil for at least one minute (three minutes at altitudes over 6,562ft) to inactivate all harmful bacteria, parasites, and viruses (CDC, 2012). Complete sterilization of water is not necessary. Although simple, boiling is not practical in many situations, including applications in a hostile environment. Additionally, boiling does not remove any pollutions or particulate contaminants, and can concentrate toxins if used extensively.

Another common water treatment method is filtration. Filtration types include carbon or activated carbon, ceramic, and reverse osmosis, among others. None of these types can remove all harmful materials individually, so all must be used in conjunction with other types of purification. The most effective filtration system is reverse osmosis. Reverse osmosis involves forcing water through osmosis, thereby passing water through a semi-permeable membrane from an area of high concentration to an area of low concentration. The most effective membranes have a pore size of 0.1 nm (CDC, 2014).

That small size is highly effective at removing protozoa, bacteria, viruses, and common chemical contaminants (CDC, 2014). Reverse osmosis systems typically include supplementary filtration before and after the membranes as well to remove particulate and sedimentary materials and chlorine. Reverse osmosis systems are one of the primary choices for the military, but current systems can be impractical mainly due to their large size and power requirements. However, these systems also strip all nutrients from the water, including nutrients necessary for human health. In fact, once in the body, the purified water can leach minerals from the body before passing (Kozisek, 2005). These factors combined render reverse osmosis, although the most effective filtration method, impractical for small, portable, POU applications.

Activated carbon absorption uses a form of granulated activated carbon charcoal with a high surface area to chemically bond with contaminants to remove them from the water. It can hold up to 50% of its weight in absorbed material (Earnest & Gressel, 2003). Activated carbon comes in different forms that vary in effectiveness, potentially removing materials ranging from only chlorine and odors to asbestos, lead, mercury, and volatile organic compounds (VOCs). However, there are many other substances and compounds it cannot remove. Therefore, it is typically used in conjunction with other purification methods.

Chemical disinfection involves adding a chemical to the water directly. Chlorine and iodine are the most common chemicals. Chlorine disinfection was first used as a primary disinfectant in Jersey City, New Jersey in 1908 (USEPA, 1999). Since then, it has been adopted worldwide. In the US in 1995, chlorine was used as a disinfectant in 64% of all community water systems (USEPA, 1999). There are some significant

advantages to using chlorine for disinfection. It is more cost effective than ozone or UV disinfection, the residual chlorine left in the water can prolong the disinfection effectiveness, it is effective against a wide range of pathogens, it can oxidize certain organic and inorganic compounds, and it can eliminate some foul odors during disinfection (EPA, 1999). Unfortunately, chlorine has disadvantages as well. For one, it is not effective against cryptosporidium (CDC, 2012). Also, the chlorine residual is toxic to aquatic life, chlorine is toxic and corrosive, causing shipping and storage concerns, it increases the total level of dissolved solids in the effluent, and the long-term effect of discharging effluent with higher levels of chlorine into the environment is unknown (CDC, 2012). Chlorine disinfection, used in combination with other treatments, is more suited for large-scale commercial purification rather than portable POU disinfection.

Iodine is the other common chemical used for disinfection. It is added typically as a tablet to drinking water and has similar disinfection properties as chlorine, to include an ineffectiveness against cryptosporidium. A unique disadvantage is that iodine effectiveness also depends on water turbidity and temperature, needing more time as the temperature decreases and turbidity increases (S. H. Clarke, 2006). Also, extended usage of iodine for disinfection can produce harmful side effects to include an enlarged thyroid (S. H. Clarke, 2006). Although iodine tablets are very portable and easy to use, there are too many drawbacks related to its effectiveness to meet the required use.

Currently there are two commercial water purification devices utilizing UV sterilization on the market in the US. Camelbak produces the All Clear^{TM} Bottle, which utilizes a mercury UV lamp with a power source in the bottle cap to sterilize water (Camelbak, 2017). The sterilization cycle lasts 60 seconds, and the user is required to

agitate the water by rotating the bottle for the cycle duration. Camelbak claims it lasts for 10,000 cycles and destroys over 99.9999% of bacteria, 99.99% of viruses, and 99.9% of protozoan cysts when used as directed (Camelbak, 2017). However, Camelbak admits that it does not work when used with turbid water, so they also sell a compatible pre-filter to remove particulate matter from the water. Camelbak also states that temperatures colder than 32 degrees Fahrenheit adversely affect the battery life due to increased fluorescent bulb heat demands, so the bottle should be warmed before use in cold environments. Furthermore, the batteries are permanently installed and can only be recharged, not replaced. Finally, Camelbak warns of hazards due to breakage and disposal of the UV lamp, as well as untreated water residue remaining on the exterior edges of the bottle.

The first company to bring UV sterilization to the portable market was Hydro-Photon with their SteriPEN®. SteriPEN® is a battery powered, wand-type, mercury-based UV sterilization device that is designed to be swirled around in a water container. Hydro-Photon claims the SteriPEN® effectively destroys over 99.99% of all bacteria, viruses, and protozoan cysts (Hydro-Photon, 2016). It can sterilize 16oz of water in 48 seconds, and 32oz in 90 seconds. It is very portable, weighing under 5 ounces. However, the SteriPEN® suffers from the same turbidity, temperature, and breakage problems as the Camelbak product.

While the inherent disadvantages of UV would remain, both of these products could be improved by adapting LED technology. The use of LEDs in place of the mercury lamps would reduce both weight and bulk, increasing portability. The lower power requirements would greatly extend the life of the products and reduce weight due

to replacement batteries. Finally, the risk of mercury contamination due to breakage would be eliminated.

Relevant Research

After establishing a practical application and useful need for UV LED water purification, it is beneficial to examine the current state of research in the field. Some of the initial research was accomplished in 2007 by Hamamoto et al. when the researchers evaluated the ability of UVA LEDs to inactivate bacteria in water (Hamamoto et al., 2007). The researchers built a reactor with eight individual LEDs producing light at a 365 nm wavelength. They also used a mercury UVC lamp as a comparison to gauge the effectiveness in terms of DNA damage of the LED reactor. The researchers found that their UVA LED reactor could successfully inactivate pathogenic bacteria in the water, however the DNA damage results were inconclusive (Hamamoto et al., 2007).

Vilhunen, Särkkä, and Sillanpää conducted further research in 2008 with their own reactors. They built two, each using ten LEDs, one at 269 nm and one at 276 nm. Both reactors mixed the water via magnetic stir plates. The researchers varied the turbidity of the water, and measured E. coli inactivation. The experimentation produced results with an inverse relationship between turbidity and inactivation. Additionally, the reactor with the 269 nm wavelength LEDs was much more efficient in terms of radiation emitted to level of inactivation than the reactor with the 276 nm LEDs (Vilhunen, Särkkä, & Sillanpää, 2009).

Chatterley and Linden conducted similar research, comparing LEDs at 265 nm to mercury lamp at 254 nm for E. coli inactivation performance (Chatterley & Linden,

2010). For the mercury lamp, they used a collimated beam apparatus. Both a batch and a flow-through prototype were created for the UV LEDs. The batch had an array of three LEDs, and the flow-through prototype had ten. The researchers found that the UV LEDs did not perform statistically differently than the mercury lamp in terms of E. coli inactivation by dosage, both in the batch and flow-through reactors, proving their viability (Chatterley & Linden, 2010).

In 2013, Oguma et al. conducted similar research with E. coli inactivation focusing solely on LEDs (Oguma, Kita, Sakai, Murakami, & Takizawa, 2013). They used both batch and flow-through reactors, along with three different wavelength LEDs at 265, 280, and 310 nm, as well as various combination pairs for the flow-through reactor. The batch reactor used a nine-LED array, while the flow-through reactor consisted of three arrays of ten LEDs each. The researchers found that the time-based efficiency was highest at 280 nm, and the fluence-based efficiency was highest at 265 nm. Another significant finding was tailing and lower inactivation efficiency in the flow-through reactor when compared to the batch with the same wavelength LEDs. Finally, the paired combination wavelength LED arrays for the flow-through reactor produced lower efficiencies than the single-wavelength arrays (Oguma et al., 2013).

One of the more recent innovations in the field has incorporated the use of Computational Fluid Dynamics (CFD) to model particle tracing, residence time, and contact time in disinfection reactors. Reactors work by ensuring each microorganism receives the necessary concentration of either chemical or UV energy. Therefore, residence time distributions, which characterize the fluid hydraulics, and contact times, which define the chemical conversion rate, are critical factors to determining a particular

reactor geometry's effectiveness (Wols, Hofman, Uijttewaal, Rietveld, & van Dijk, 2010). In certain reactors, there is a distribution of contact times, meaning each microorganism receives different doses. Therefore, characterizing then optimizing the fluid flow to ensure minimum contact time becomes critical. As such, the mean residence time becomes an important reactor characteristic, as it describes that contact time and becomes a measure of reactor efficiency. B. A. Wols et al. (2010) used a finite element analysis software called Finlab to model an ozone contactor. Their model was able to produce predictions of flow fields, ozone concentration fields, residence time distributions, particle trajectories, ozone exposure (CT value), and inactivation levels. The researchers found that the particle tracing method most accurately reproduced the actual movements of individual microorganisms in the contactor. By accurately predicting the particle behavior, they were able to conclude that improving the hydraulics of the contactor had a significant impact on disinfection (Wols et al., 2010).

Recognizing CFD modeling's powerful potential, Chen, Deng, and Kim (2011) developed a model designed to replicate a UV lamp reactor, specifically in the areas of fluence rate, flow field, and microbial inactivation. The researchers' model incorporated all three elements while focusing on the hypothesis that light reflected by the reactor's walls has an effect on inactivation. Using Ducoste, Liu, and Linden's work from 2005 to validate their model, Chen et al. found good agreement between the modeled reactor's results and the laboratory results with regards to fluid flow and microbial log inactivation. Additionally, the researchers discovered higher fluence rates near the reactor walls, supporting their reflection hypotheses (Chen, Deng, & Kim, 2011). These modeling

results, validated by real fluence, fluid flow, and microbial inactivation data, demonstrate the efficacy of modeling and simulation in this application.

In an alternate but related application, Wang et al. incorporated the use of UV LEDs into a CFD model, albeit of a photocatalytic odor abatement process using a continuous reactor (2012). Their model incorporated two main elements—a radiation field model to simulate the radiation characteristics and reaction kinetics of UV LEDs, and CFD model to recreate the fluid flow elements, although this time simulating air flow rather than water. The model was able to calculate the advection, diffusion, and chemical reactions within the reactor while demonstrating the impact of the LEDs' geometric array on the reactor performance (Wang et al., 2012).

Another related application of CFD modeling is in the field of bioreactors, which are used to distribute nutrients within porous materials. Lawrence, Devarapalli, and Madihally (2009) examined the relatively unknown field of fluid dynamics within a large porous structure as implemented in such bioreactors. The researchers used COMSOL Multiphysics® Modeling Software to model the effect of reactor geometry on fluid distribution characteristics. They created two different reactor geometries, one rectangular and one circular, and altered each with three different inlet and outlet conditions. The flow was characterized by the residence time distribution (RTD) in attempt to identify potential non-ideal flow conditions such as channeling and dead zones. The researchers conducted laboratory experimentation on the physical reactors in the same configurations in order to validate the model results. Finally, both the model and experimental iterations were accomplished both with and without the porous media in place. The researchers found that unlike the rectangular reactor, the circular reactor

produced “secondary circulations in the flow field” (Lawrence et al., 2009), which increased the non-ideal flow fields, leading to more channeling effects. Additionally, the researchers found that the elastic nature of the porous material resulted in a compression effect in the laboratory experiment, but the model was not able to recreate such effect. That compression produced lower RTD times as the channeled flow under a higher pressure exited the reactor sooner than the flow in the unpacked reactor. Overall, the researched produced good agreement between the RTDs of the model and experimental data.

Further research utilizing COMSOL Multiphysics® was accomplished by Cruz-Diaz et al. in 2014 on the FM01-LC parallel plate reactor with the objective of discovering more efficient inlet and outlet distributer geometries by analyzing RTD curves at varying flow rates (Cruz-Díaz, Rivero, Almazán-Ruiz, Torres-Mendoza, & González, 2014). The FM01-LC reactor with parallel plates is a continuous flow, electrochemical reactor, popular for its use in laboratory experiments. The researchers conducted two sets of laboratory experiments with the reactor, the first with the original inlet and outlet geometries, and the second with new geometries at seven different flow rates from 0.5 L/min to 3.5 L/min. In terms of RTD, the researchers found that as the flow rate increased, the experimental RTD more closely matched the theoretical RTD as the tailing phenomena decreased for both reactor geometries, but the new geometry reactor exhibited trends more closely related to plug flow than the original geometry. Additionally, the researchers found the model produced average residence times with only small differences from the experimental residence times, indicating accurate simulation results. Overall, the new geometry reactor produced flow fields that were

more homogeneous over the entire reaction zone than the original geometry reactor according to the CFD results (Cruz-Díaz et al., 2014).

Finally, Jenny, Simmons III, Shatalov, and Ducoste used COMSOL Multiphysics® Modeling Software to model a continuous flow UV LED disinfection reactor (2014). The researchers replicated the physical geometry of an existing reactor in the software, then added the relevant physics characteristics which included hydraulic fluid flow, fluence, and microbial inactivation. In the laboratory, the researchers conducted tracer tests using a sodium chloride solution, measuring the effluent concentration via conductivity analysis. The fluence rate was characterized by using chemical actinometry, wherein concentrations of potassium iodide, potassium iodate, and borax were exposed to UV light in the reactor at two different flow rates, thereby forming triiodide, the concentration of which was then measured by spectroscopy. Finally, the researchers tested microbial inactivation using the bacteriophages MS-2 and Qβ, which represent common viruses (Jenny et a., 2014).

In validating the model data, the researchers began by characterizing the both the experimental and model data. The researchers qualitatively compared the concentration curves and quantitatively compared the hydraulic residence times (HRT) and level of axial dispersion using the dispersion coefficients. The dispersion model attempts to characterize reactors that are under neither true plug flow nor completely mixed conditions (Levenspiel, 1999). The dispersion coefficient (D) describes the amount of diffusion-like spreading of the tracer process. The D coefficient can be calculated by minimizing the sum of squared error (SSE) between a theoretical density function from

the plug flow dispersion model (Equation 1) and the experiment or model-produced residence time density function (Jenny et al., 2014).

$$\left(\frac{1}{\left(2(\pi \cdot \theta \cdot D)^{.5} \cdot HRT\right)} \right) \exp\left(- \frac{(1-\theta)^2}{(4 \cdot \theta \cdot D)} \right) \tag{1}$$

In this equation, θ represents the ratio of observed time to HRT. A D coefficient of zero indicates true plug flow with no spreading, a small D coefficient indicates slow spreading, and a large D coefficient indicates rapid spreading (Levenspiel, 1999). Tracer curves are sensitive to irregularities in flow (eddies, dead zones, bypassing, etc.), so any abnormality can have a large impact on the D value. If the reactor geometry is producing dead zones, for example, a reduction factor can be applied to the HRT in an attempt to more closely match the curves and produce a more accurate D value.

In Jenny et al.'s research, the RTD functions from the hydraulic tracer test produced a good agreement (within 3% deviation) between theoretical and experimental hydraulic residence times (2014). Additionally, there was a 3% deviation between the model and experimental data at 190 mL/min and 6% deviation at 109 mL/min. With regards to fluence rate, the model data differed from the experimental data by 8.9% to 22.83% at different combinations of LED array configuration and flow rate. Finally, the higher flow rate produced a more accurate model for bacterial inactivation compared to the lower flow rate (Jenny et al., 2014).

Jenny et al.'s work provides the most accurate roadmap to this research. The experimental methods and model validation, specifically the hydraulic tracer tests and fluid flow model, are very similar to the methods employed to examine the current AFIT reactor. Although the AFIT reactors utilize significantly lower flow rates than the

aforementioned research, the results are still positive with regards to model validation and eventual prototype optimization.

Locally, UV LED reactor research has been underway at AFIT since 2013 (Spencer, 2014). There have been a number of different prototypes designed and constructed, using different configurations of geometric design, material type, and LED power and array. Drew Gallucci (2016), was the first to introduce modeling utilizing the COMSOL Multiphysics® Modeling Software. He used the software to characterize the fluid flow at different flow rates in his prototype reactor. Finally, Shandon James (2017) is conducting concurrent research also using COMSOL Multiphysics® to model different reactor prototypes that also incorporate the ray optics physics elements.

III. Methodology

The purpose of this chapter is to review the methods used to answer the research questions in Chapter 1. COMSOL Multiphysics® Modeling Software was used to develop the model referenced in questions one and two, and a set of laboratory experiments was used to address question three. The modeling was conducted in an iterative process, building from basic, rudimentary models with single physics characteristics to more complex versions with multiphysics couplings. The laboratory experiments were conducted with the PTFE reactor developed by Drew Gallucci (2016). Gallucci's reactor is a modular design with different end caps, each producing a different flow characteristic. The end caps on the reactor used produced a perpendicular flow profile, characteristics of which will be discussed in Chapter 4.

Laboratory Experiment

The overall process involved filling the reactor with deionized (DI) water, injecting the dye, then pumping more DI water through the reactor until the concentration returns to zero. Pump flow rates of 1mL/min, 2mL/min, 4mL/min and 8mL/min were used. Figure 1 shows the overall experimental layout.

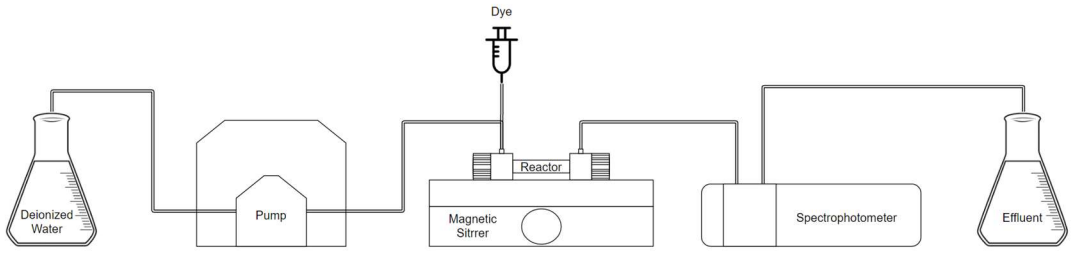

Figure 1. Laboratory Experiment Layout

The base solution with which the dye was mixed was deionized (DI) water. The flow rates were relatively low for all iterations of the experiment, so enough DI water for each iteration could be stored in a beaker. A length of Masterflex EW-06508-14 flexible tubing with an interior diameter of 1.6mm brought the DI water from the beaker to the Masterflex pump (model 77200-50, Cole-Parmer, Gelsenkirchen, Germany). The tubing continued through the pump and was attached to the inlet nozzle of the reactor. The reactor lied horizontally on a Fisher 14-522-2 magnetic stir plate. Although not active in this experiment, the stir plate served as a resting platform to locate the reactor near the spectrophotometer.

That same tubing ran from the reactor outlet nozzle to the .39 mL cuvette in the spectrophotometer. The concentration was measured using an Agilent Technologies Cary 60 UV- Vis Spectrophotometer (Santa Clara, CA). The Spectrophotometer used a 620-630nm wavelength light to measure the absorption of the dye as the water passed through the cuvette. The adjustable reading frequency for the 8 mL/min, 4 mL/min, and 2 mL/min conditions was adjusted to one-tenth of a minute. A frequency of two-tenths of a minute was selected for the 1mL/min condition. More tubing allowed the water to flow out of the spectrophotometer and deposited it in a separate effluent beaker. Figure 2 shows an image of the experimental layout.

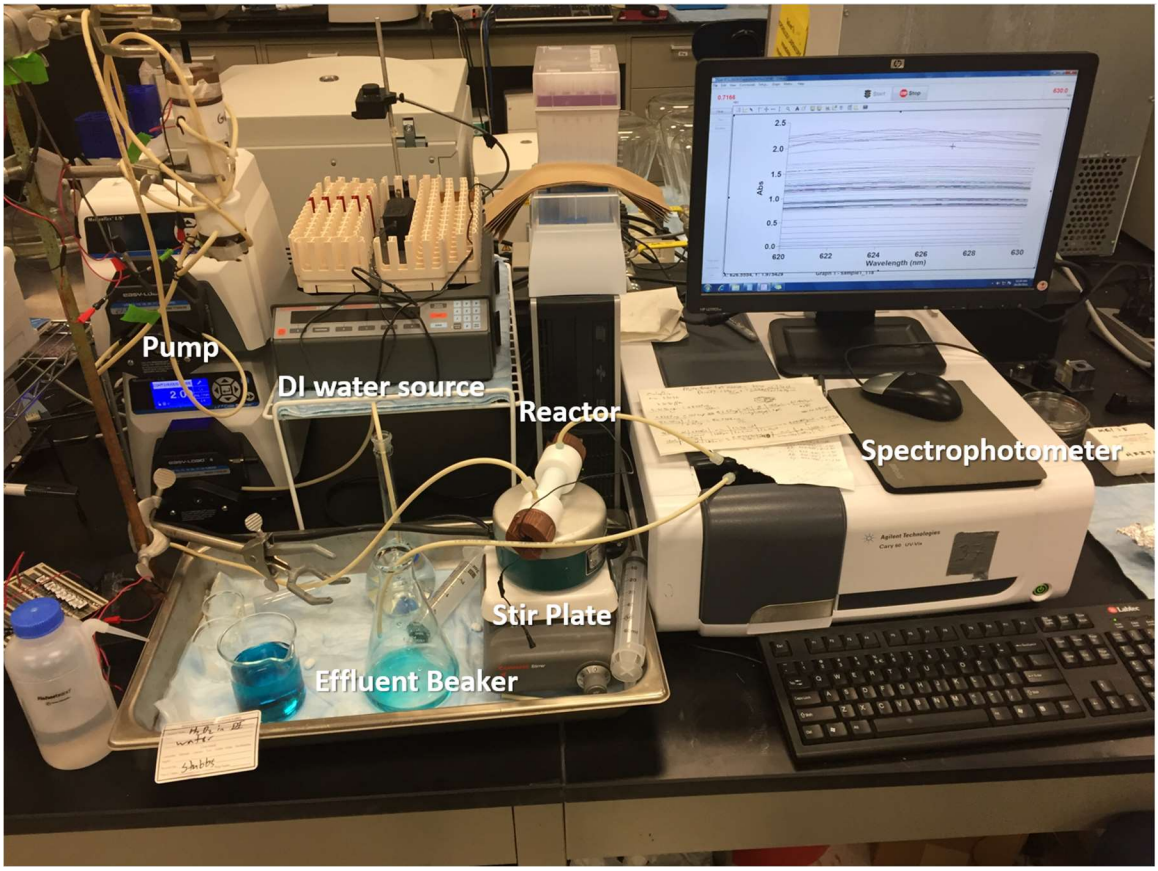

Figure 2. Image of Laboratory Experimental Equipment

To begin each experiment iteration, the system was pre-filled with DI water and the spectrophotometer was zeroed. The pump was set at the desired flow rate and activated. A dye solution was created by mixing 75µL of Fast Green FCF dye (molecular weight: 808.843g/mol) with 800µL of DI water and prepared in a syringe. This produced a starting concentration of 0.4285 mol/m^3 or 346 parts per million (ppm) of dye, and equated to a concentration of 1 mM/L within the reactor. Once the water was flowing through the reactor, the inlet tube was removed from the reactor and the syringe was attached. The dye solution was injected into the reactor at a rate of approximately 3mL/min. Once all the dye was injected, the inlet tube was reattached and the

spectrophotometer was activated. Based on historical data, it took approximately four reactor volumes of liquid (160 mL) to pass through the system until the absorbance returned to zero. For the 1mL/min flow rate, it was achieved in approximately three hours while at 8mL/min it was achieved in about 26 minutes. Once the absorbance approached zero, the system was shut down and the data was stored.

Model

The geometry construction, meshing, physics settings, solving, and post processing was all completed utilizing COMSOL Multiphysics® Modeling Software (version 5.2a, COMSOL, Inc., Burlington, MA). First, the interior geometry of the reactor, inlet, and outlet tubes was constructed and assigned the material properties of water. The outlet tube was modeled at 20cm long, matching the distance between the reactor and spectrophotometer in the lab. Figure 3 displays the full model, and Figure 4 provides a detail of the reactor. The scale for both figures is in meters.

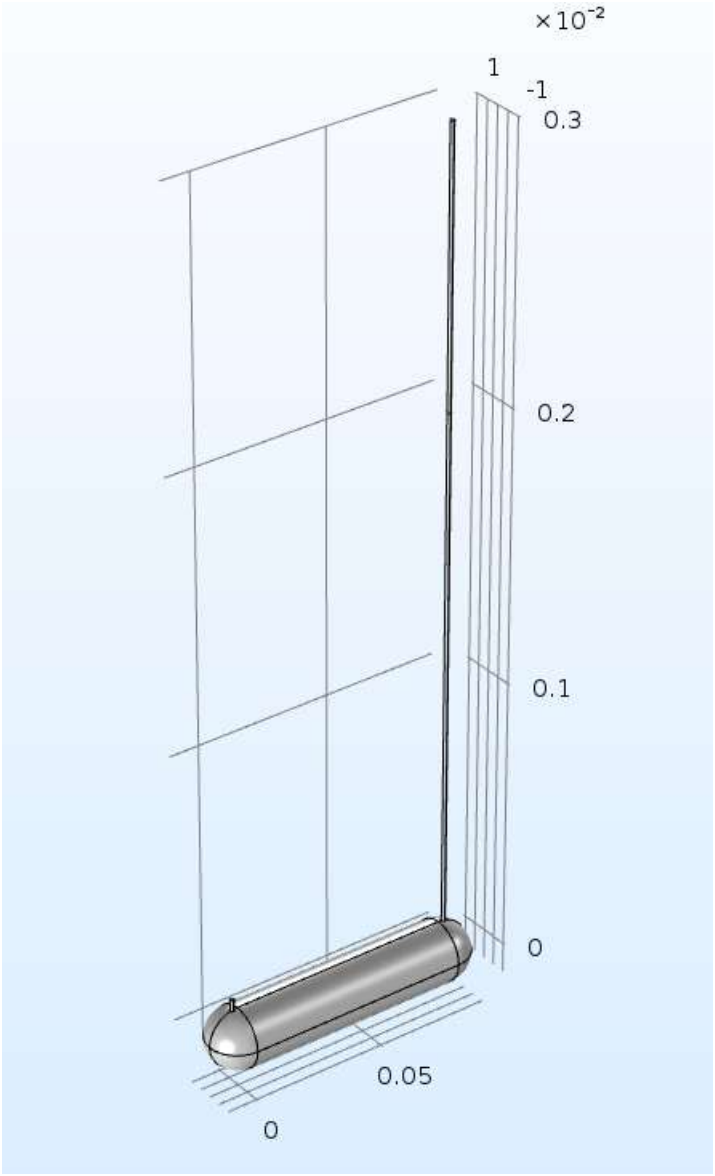

Figure 3. Full Model

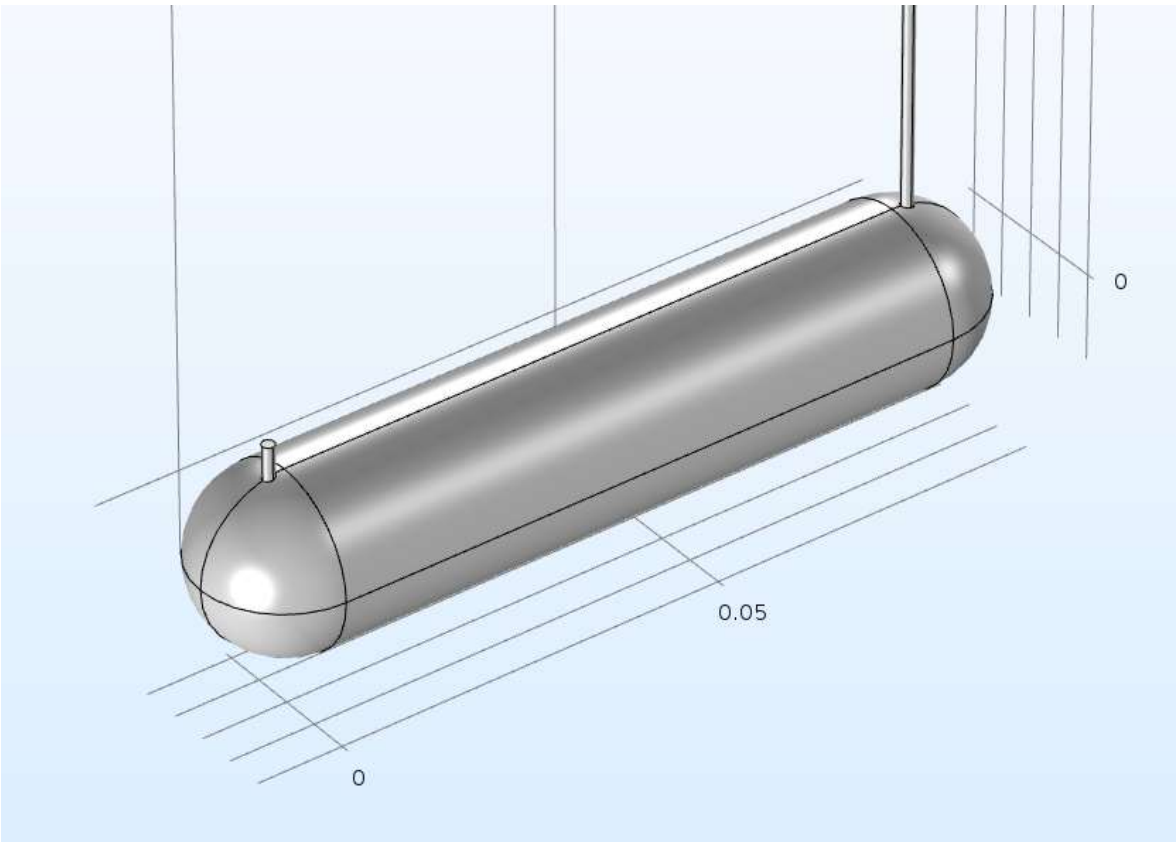

Figure 4. Reactor detail

Once the geometry was complete, the inlet and outlet tubes were then meshed with “finer” triangular elements, the reactor body with “fine” tetrahedral elements, and were then optimized for fluid dynamics. This produced 336,037 elements over the entire domain. Meshing to a higher refinement produced no significant changes in results. Figure 5 shows the meshed model of the reactor, and Figure 6 shows the inlet tube detail.

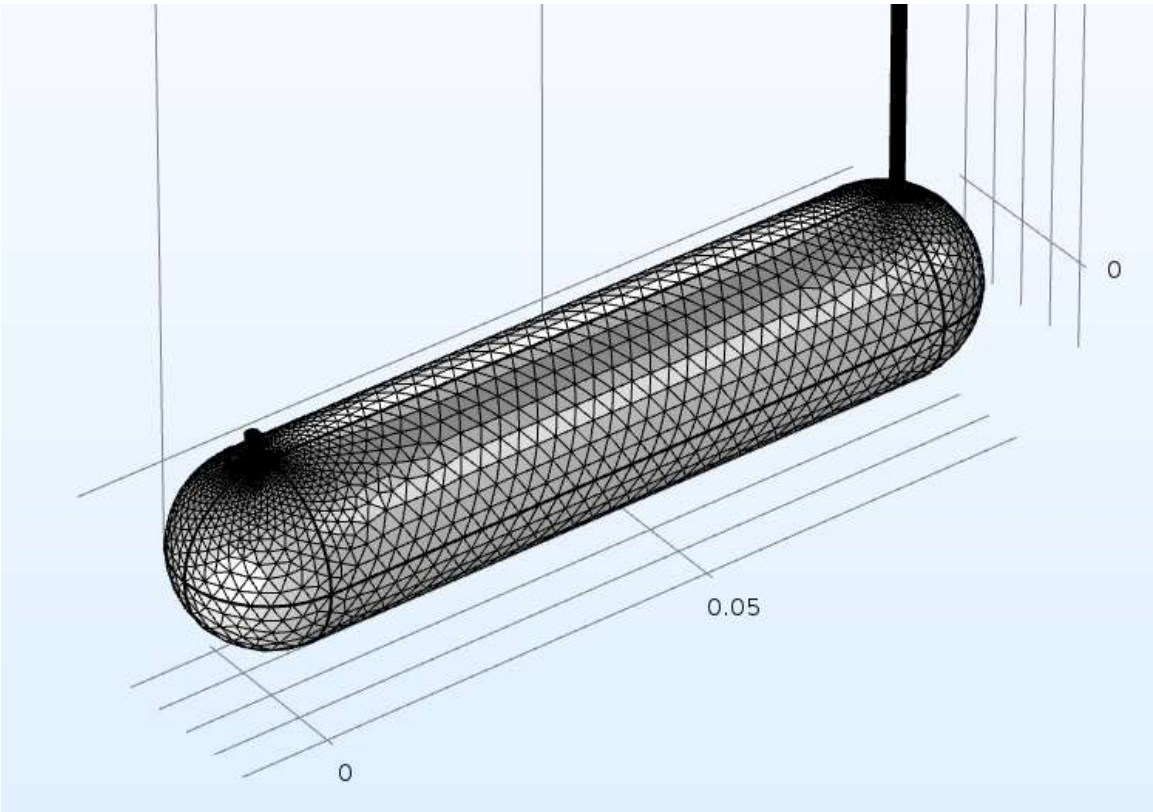

Figure 5. Reactor Mesh Detail

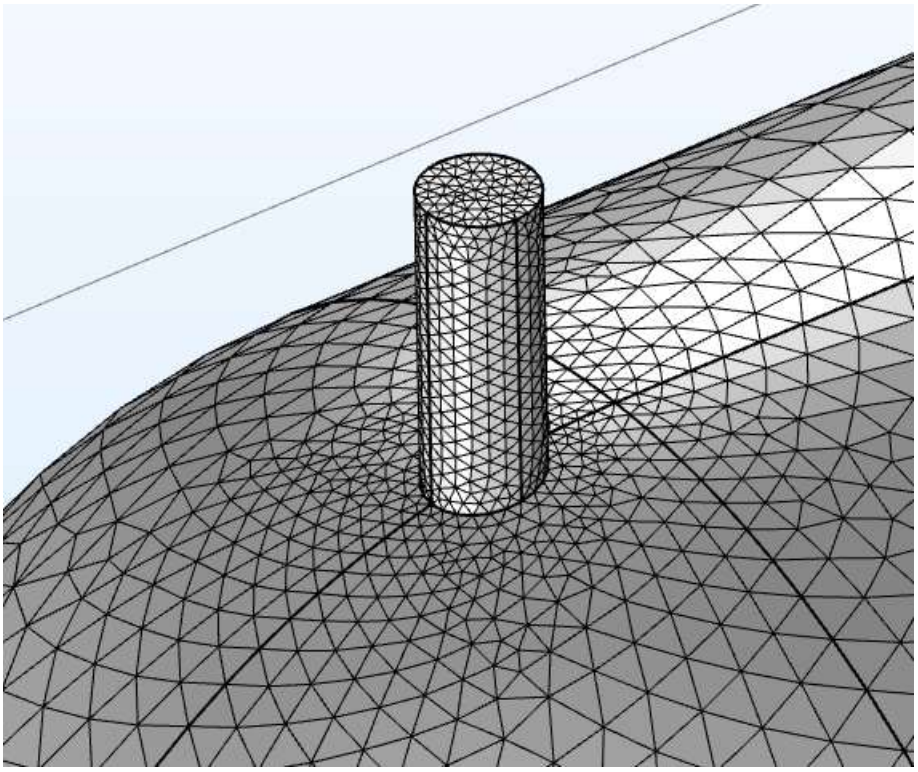

Figure 6. Inlet Tube Mesh Detail

Next the fluid flow physics package was applied to the model. This package created the fluid flow profile and output both pressure and velocity. It solved the Navier-Stokes laminar flow, or conservation of momentum equation, and the continuity, or conservation of mass, equation, which are, respectively:

$$\rho(\mathbf{u}\cdot\nabla)\mathbf{u} = \nabla\cdot\left[-p\mathbf{I}+\mu\left(\nabla\mathbf{u}+(\nabla\mathbf{u})^{T}\right)-\frac{2}{3}\mu(\nabla\cdot\mathbf{u})\mathbf{I}\right]+\mathbf{F} \quad (2)$$

$$\nabla\cdot(\rho\mathbf{u}) = 0 \quad (3)$$

The inlet boundary condition was specified at the reactor inlet tube, and the inlet velocity was established as a laminar flow at either 8 mL/min, 4 mL/min, 2 mL/min or 1

mL/min. The software accounted for a pre-established laminar flow profile (having traveled .5 m in this case), negating the need to use a long inlet tube as was applied in the actual experiment. The velocity at the inlet was constant across the diameter, and the outlet tube was assigned a zero-pressure boundary condition. The inlet tube, outlet tube, and reactor walls were given the no-slip boundary condition, representing zero fluid velocity at the fluid-solid interface.

The other physics package applied was transport of diluted species. This package incorporated the flux due to diffusion to account for the concentration gradient between the dye and the water, as governed by Fick's first law, which states the molar flux due to diffusion is proportional to the concentration gradient. It solved the convection diffusion equation shown below:

$$\mathbf{N}_i = -D_i \nabla c_i + \mathbf{u} c_i \tag{4}$$

A concentration inflow boundary condition was set at the inlet tube and the velocity was assigned the velocity profile from the laminar flow physics. The concentration was assigned to a rectangular function, which essentially turned off the flow of dye into the reactor at the appropriate time to achieve the desired 875 μL quantity. The dye concentration was set at 0.4285 mol/m^3. The outflow boundary condition was established at the outlet tube.

Once the geometry is established and meshed and the physics equations are applied, COMSOL Multiphysics® solves the equations in studies, which can be either stationary or time dependent. The analysis was broken up into two studies to reduce

computational time and requirements. The first study was stationary, or performed at steady-state, and calculated the laminar flow velocity variable and pressure variable in the reactor. The second study was time dependent, or transient, and calculated interaction between the dye and water in the reactor, considering both convection and diffusion. The study used the velocity profile established by Study 1 as the basis for the convection elements, and a diffusion coefficient measured at 3.9E-10 m^2s^{-1} for Fast Green FCF to establish the diffusion across the concentration gradient and calculate the concentration variable (Werts et al., 2012). The study was set to calculate its variable every hundredth of a minute, or every 0.6 seconds, but only output every tenth of a minute or 6 seconds to match the laboratory experimental data. The exception is the 1 mL/min flow rate, as the experimental data was recorded every two-tenths of a minute, or every 12 seconds. The model output again matched that time interval, but the model calculation interval was still 0.6 seconds. The overall duration of the study also matched the laboratory results for each respective flow rate.

Concentration, the most relevant output variable, was initially calculated as a surface average across the end of the outlet tube. However, a more accurate method was implemented by extending the length of the outlet tube by 20 mm to duplicate the 0.39 mL volume of the cuvette then taking the concentration as a volume average over that length. The concentration over time data produced by both the experiment and the model is the main source of data used in the comparison between the experimental and model results. The data was compiled and exported in a table. Additionally, the model was able to produce a series of graphics to show the interior concentration levels at different points in time.

IV. Results and Analysis

Chapter Overview

This chapter reports and discusses the results of the laboratory experiment and the COMSOL Multiphysics® model.

Laboratory Experiment Results

The spectrophotometer returns results as the valueless absorbance amount, so it has been converted to ppm based on the dye's physical properties for clarity and ease of use. The laboratory results for all flow rates are reported together below in Figure 7. Individual concentration output curves are reported in Appendix A.

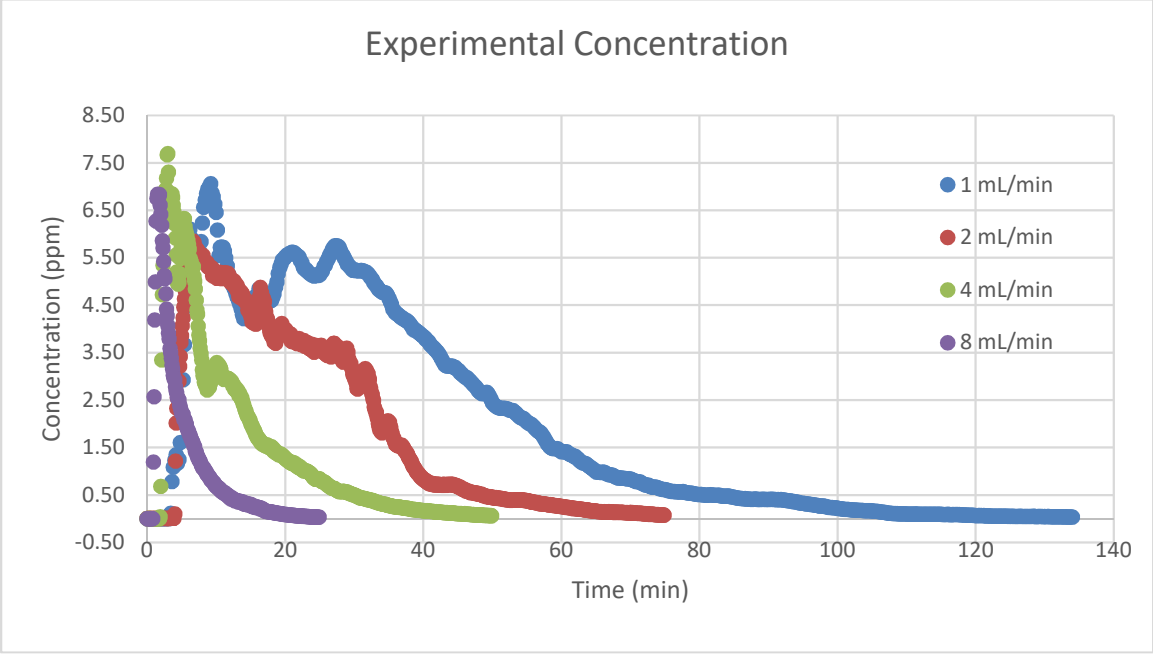

Figure 7. Experiment Concentration Output

The dye is relatively dense, so at lower flow rates areas of higher concentration were undisturbed by convection and therefore pass through the reactor without mixing. However, lower flow rates also lead to a higher likelihood of diffusion, so that may lead to lower peak concentration values. Conversely, higher flow rates create more mixing that in turn produce a more steady and predictable degradation curve. Additionally, as described in Chapter 3, the dye is inserted manually by syringe. Uneven pressure on the syringe may have led to the initial spike visible in the 1 mL/min curve, creating an artificially high concentration level.

For 1 mL/min, the theoretical residence time, calculated from the reactor volume and water flow rate, was 40.8 min. The experimental data produced a residence time of 35.06 min, which results in a 14.08% difference from the theoretical time. The concentration peaks at 7.06 ppm, occurring at 9.2 min, and approaches zero at approximately 124.2 min. Of note is that the concentration measurements were recorded every two-tenths of a minute for this iteration, vice one-tenth for all subsequent flow rates.

The 2 mL/min condition avoided the initial spike in concentration, but displays an unusually gradual degradation curve to include the density related spikes. The more gradual curve produces a residence time that is higher than the theoretical at 21.5 min vice 20.2 min, a 5.14% difference. The concentration peaks at 5.85 ppm at 6.6 min, and approaches zero at approximately 74.9 min.

The 4 mL/min iteration returns to a more standard degradation curve, but maintains the variation present in the previous iterations. The experimental residence time is 13.98% different from the theoretical residence time at 11.86 min and 10.2 min,

respectively. The concentration reaches a maximum of 7.69 ppm at 3 min, and returns to zero at approximately 49.9 min.

Lastly, the 8 mL/min flow rate produces the best degradation curve, most likely due to the convection driven mixing caused by the higher flow rate. The residence time is 5.07 min, which is 0.59% different from the theoretical time of 5.1 min. The maximum concentration of 6.84 ppm is reached at 1.5 min, and the concentration approaches zero at approximately 22.3 min. Table 1 below summarizes these results.

Table 1. Experimental Data Summary

	Theoretical Residence Time (min)	Calculated Residence Time (min)	Theoretical Residence Time Difference (%)	Peak C (ppm)	Peak C Time (min)	Zero C Time (min)
1 mL/min	40.8	35.06	14.08	7.06	9.2	124.2
2 mL/min	20.4	21.5	5.14	5.849	6.6	74.9
4 mL/min	10.2	11.86	13.98	7.69	3	49.9
8 mL/min	5.1	5.07	0.59	6.84	1.5	22.3

COMSOL Multiphysics® Model Results

The modeling results are broken into three categories for each flow rate, beginning again with 1 mL/min. The first two correspond with each of the two studies conducted in the model, and the third produces the concentration over time data that will be analyzed and compared to the experimental data.

1 mL/min Modeling Results, Analysis, and Comparison

As mentioned in Chapter 3, Study 1 in each model produced the stationary velocity profile of the reactor and inlet and outlet tubes. To characterize and visualize the fluid velocity and path, two different types of outputs are reported utilizing a cross-sectional multislice and streamline graph in Figures 8 and 9 respectively. In each,

velocity increases in magnitude (reported as m/s) as color gradient moves from blue to red.

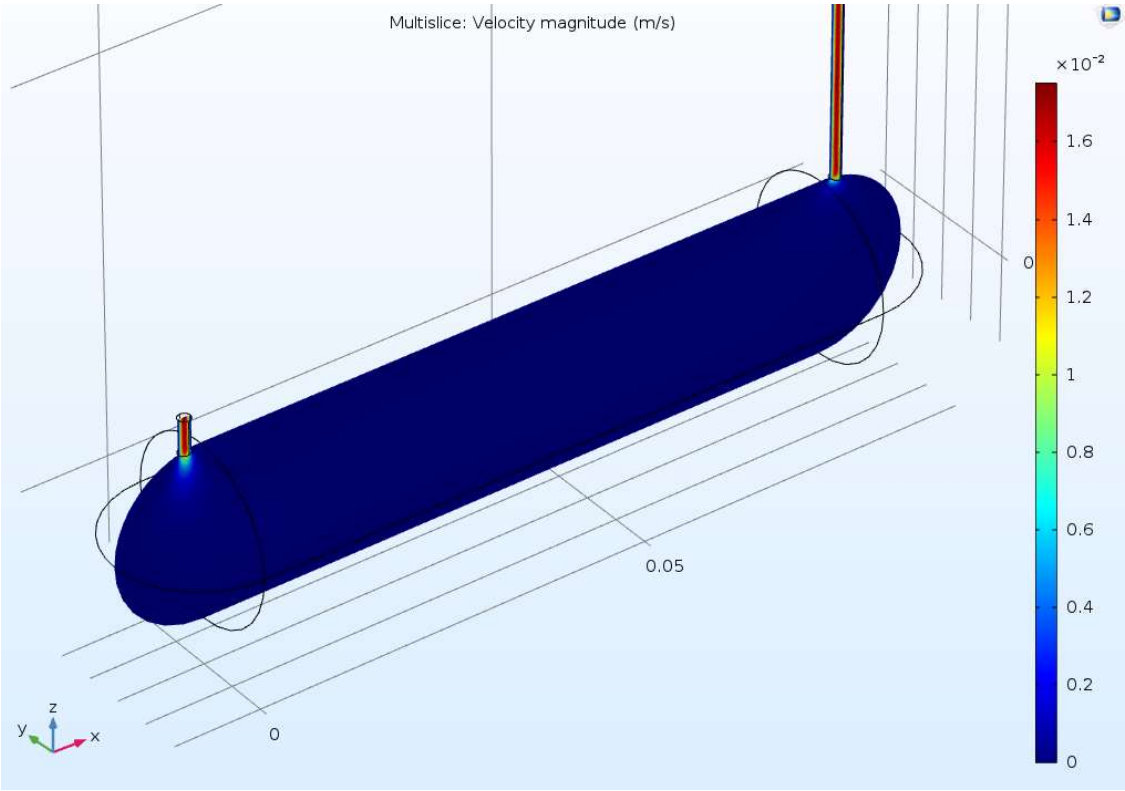

Figure 8. 1 mL/min Velocity Magnitude (m/s) Multislice

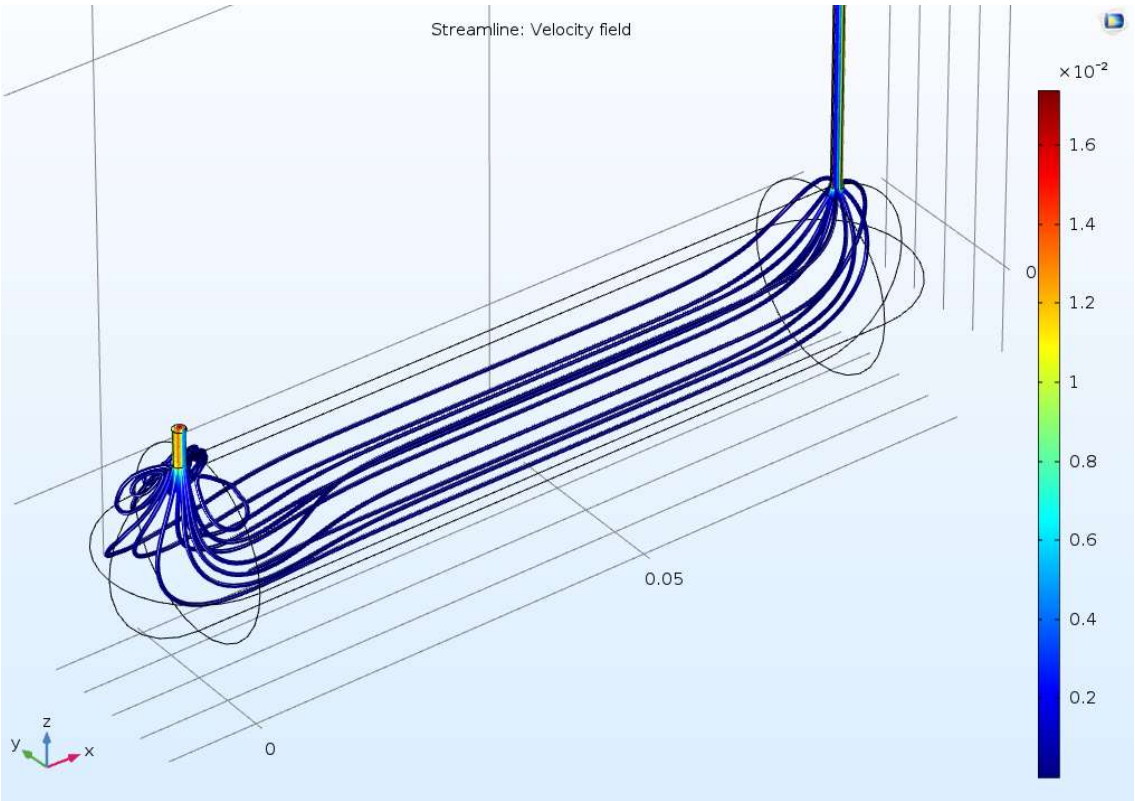

Figure 9. 1 mL/min Velocity Magnitude (m/s) Streamline

Note the velocity is relatively low throughout the reactor, with the exceptions at the inlet and outlet tubes. There are some vortexes visible in the velocity field that may either contribute to mixing or create dead zones, but are considerably fewer than the subsequent higher flow rates.

Study 2 produces the concentration over time data. The slice concentration graphs are combined in one figure (Figure 10) to show the movement of the dye concentration through the reactor over time. The concentration is reported in mol/m^3 and the color gradient again indicates increasing concentration as the color moves from blue to red. The concentration inflow is located at the inlet pipe and is only active for the appropriate amount of time to meet the 875 µL volume of dye.

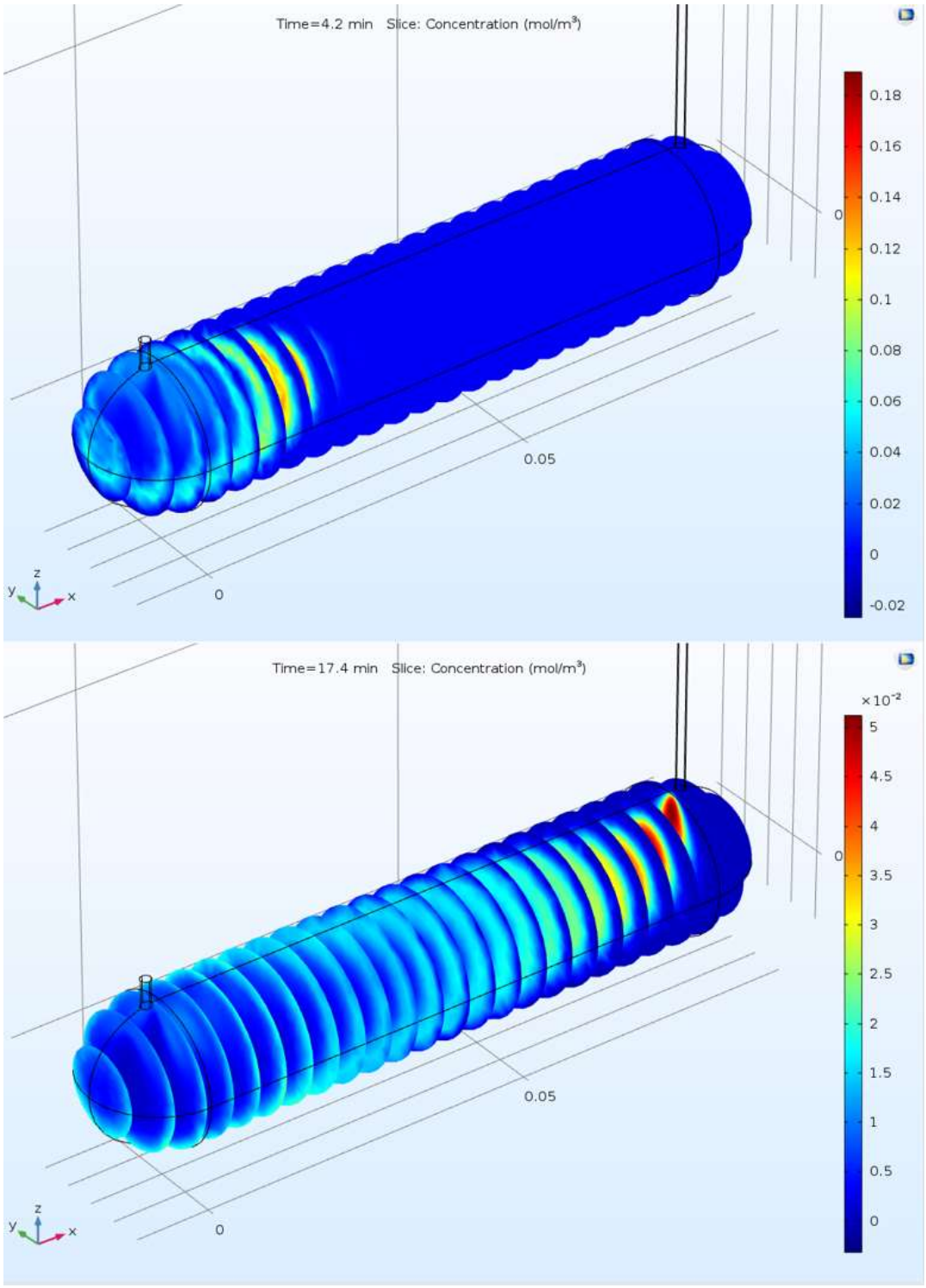

Figure 10. 1 mL/min Slice Concentration at 4.2 min and 17.4 min

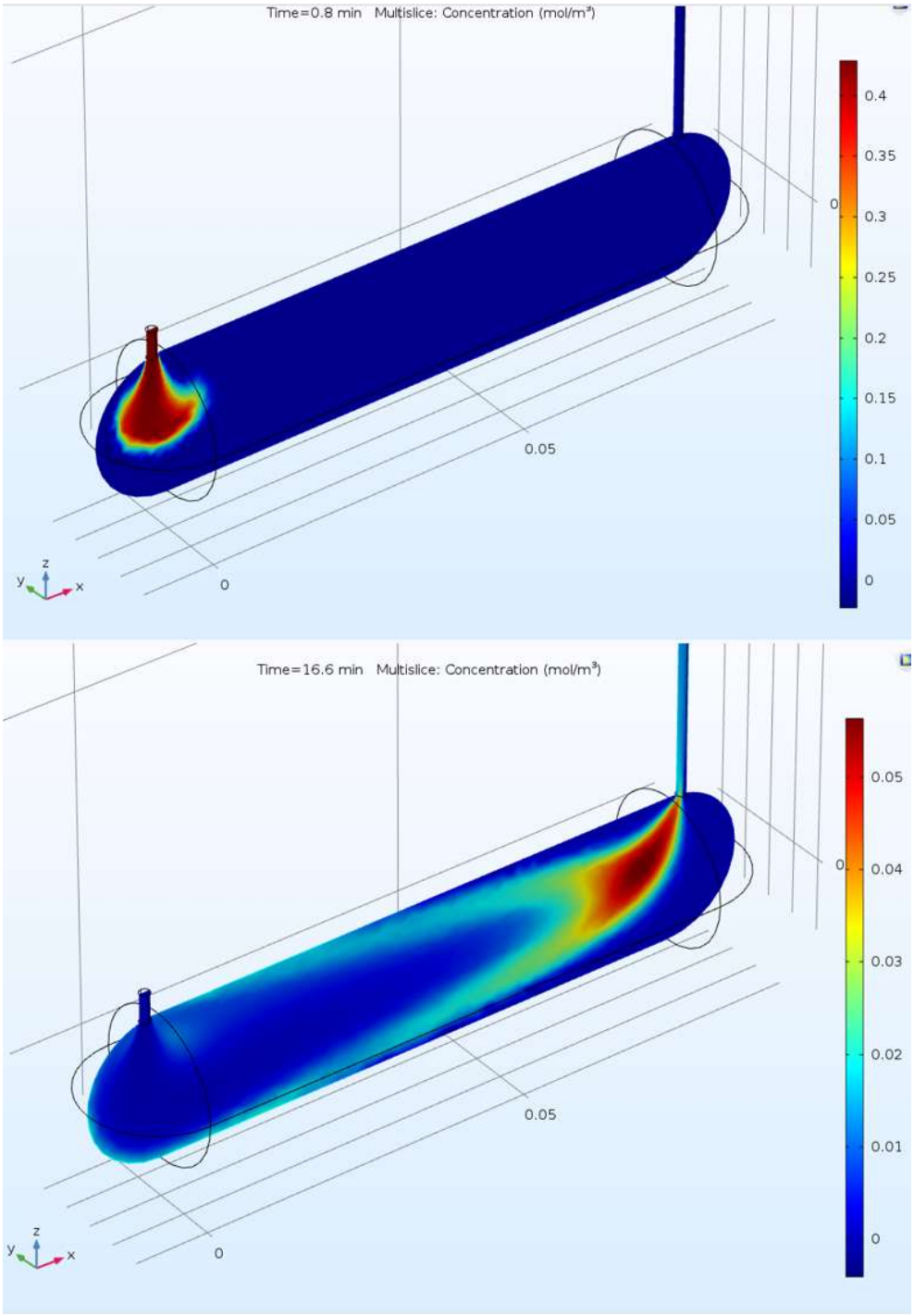

Figure 11. 1 mL/min Multislice Concentration at .8 min and 16.6 min

A similar comparison is shown in Figure 11, this time utilizing a multislice graph at different time intervals to show the dye entering and leaving the reactor.

Those particular intervals were selected to portray the dye's characteristics as it transitions through the reactor. The concentration output was measured as the average concentration over a volume of the outlet tube equating to the size of the cuvette in the spectrophotometer. The concentration over time is shown in the chart below, Figure 12.

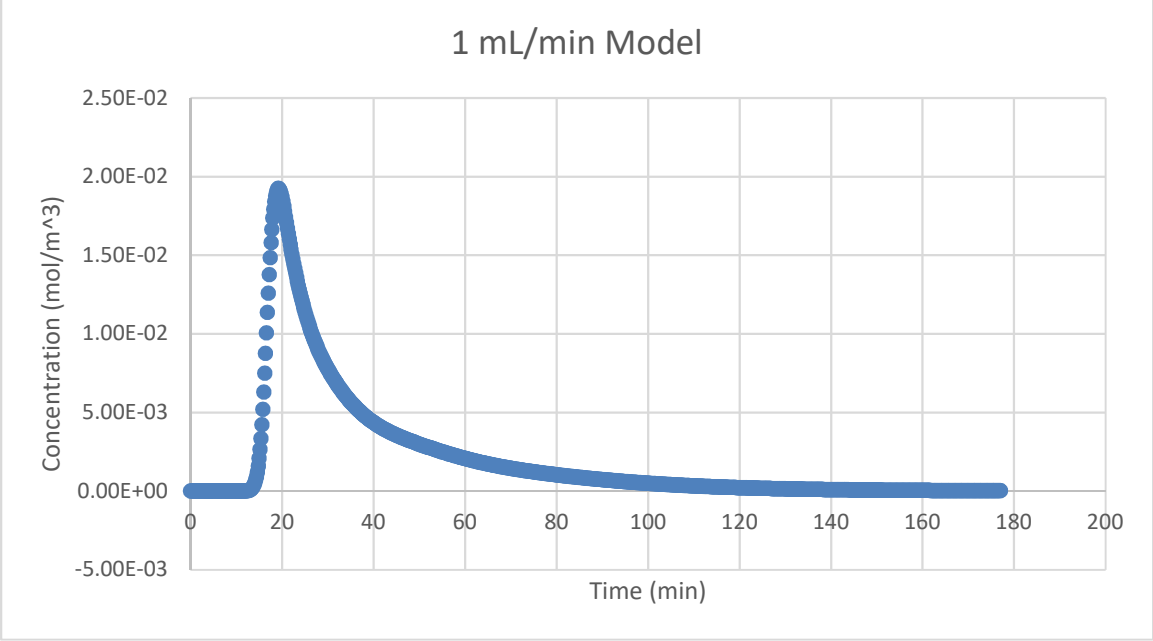

Figure 12. 1 mL/min Concentration

The concentration peaks at 0.0197 mol/m^3 at 19.6 min and reaches zero at approximately 148.8 min. The residence time is 38.71 min, which is 5.1% different from the theoretical time of 40.8 min. In order to directly compare concentration values, the curves must be normalized as the model and experimental data produce concentrations with different units. Taking each concentration value as a percentage of the initial concentration puts the data on the same scale and can be overlaid and compared. Figure 13 shows the concentration curves for the model and the experiment on the same chart.

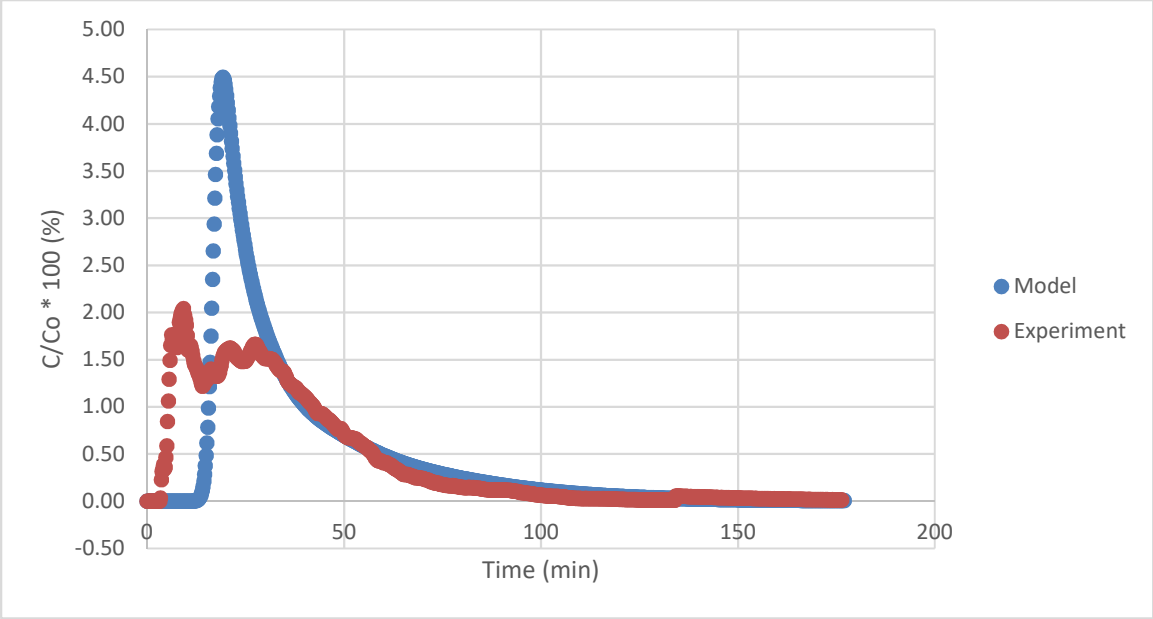

Figure 13. 1 mL/min Model and Experimental Concentration

Qualitatively, the curves share some similarities and differences in shape. The peaks are different, but the slopes of the degradation curves are similar. Quantitatively, the model curve peaks later at a much higher percentage (19.6 min and 4.60% respectively) than the experiment (9.2 min and 2.04%), but the curves reach zero at somewhat similar times-124.2 min for the experiment and 148.8 min for the model. The residence times are 10.41% different, with the model at 38.71 min and the experiment at 35.06 min.

2 mL/min Modeling Results, Analysis, and Comparison

As the flow rate increases, the overall duration shortens and the concentration peak beings to decrease. Figure 14 shows the fluid flow velocity magnitude profile and Figure 15 shows the velocity streamlines, now at 2 mL/min, from Study 1 of the model.

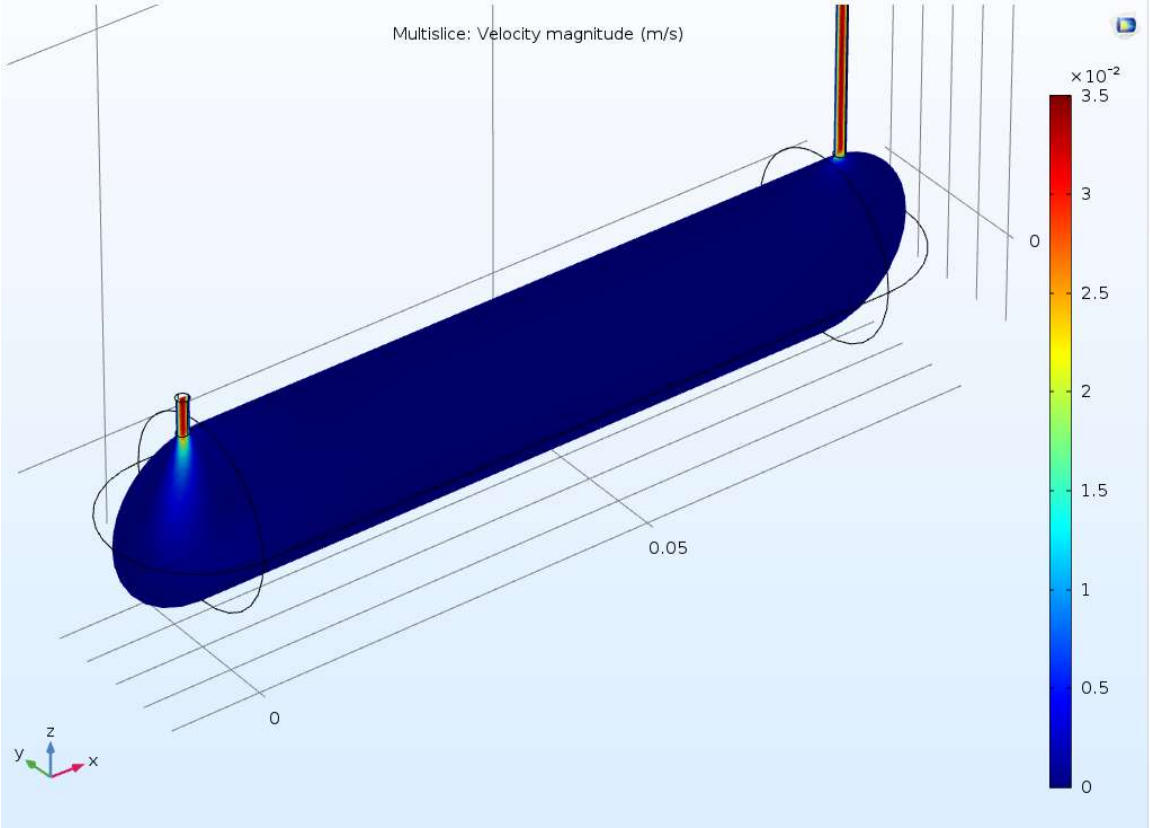

Figure 14. 2 mL/min Velocity Magnitude (m/s) Multislice

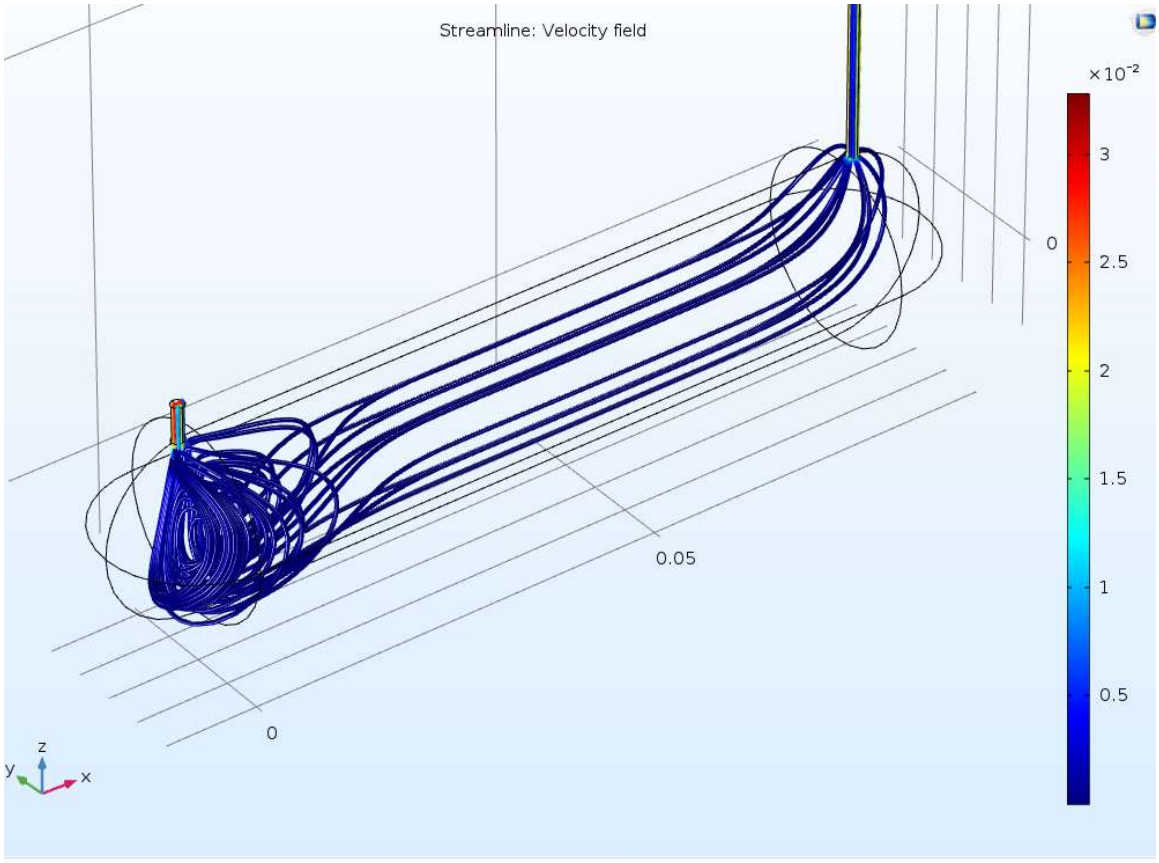

Figure 15. 2 mL/min Velocity Magnitude (m/s) Streamline

The multislice graph appears similar to 1 mL/min with very low flow rates in the reactor, but the streamline graph reveals much more mixing at the inlet. Study 2 produces the concentration, show in Figure 16 at two different time iterations.

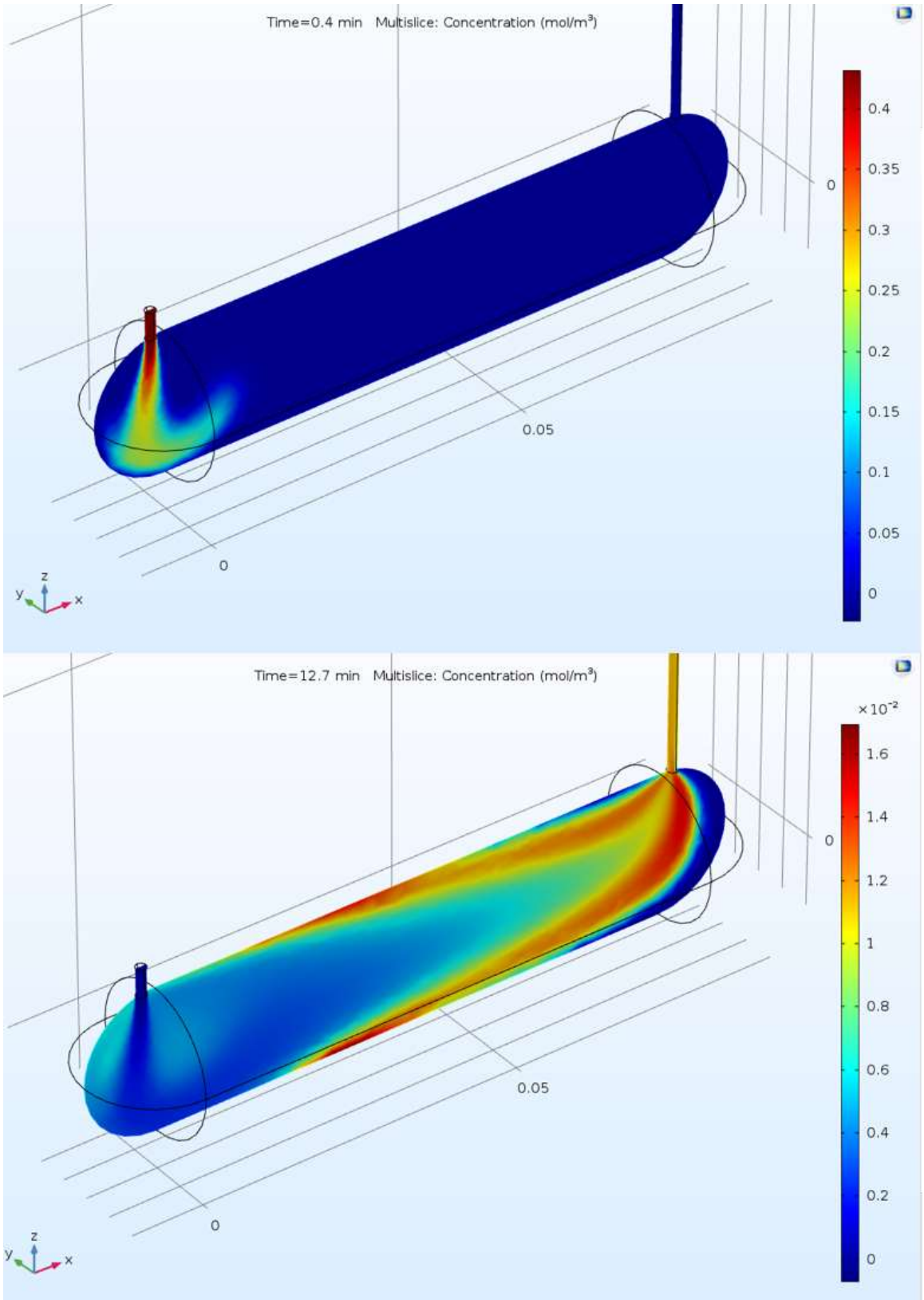

Figure 16. 2 mL/min Multislice Concentration at .8 min and 16.6 min

Comparing the scale on the 2 mL/min multislice to the 1 mL/min reveals the lower concentration values in the 2 mL/min model as the dye moves through the reactor, however the larger areas of higher concentration in Figure 16 also illustrates increased mixing of the dye as the flow rate increases from 1 to 2 ml/min. Figure 17 provides the concentration volume average over time.

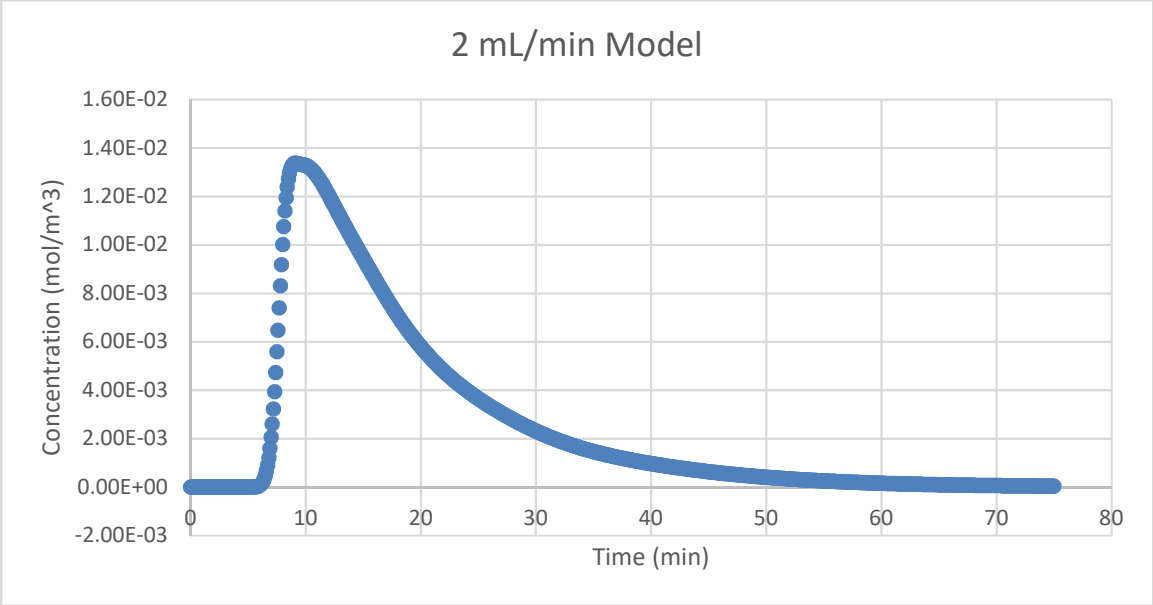

Figure 17. 2 mL/min Concentration

The concentration peaks lower at .013 mol/m^3 at 9.6 min and reaches zero at approximately 68.8 min. The residence time is 19.04 min, which is 6.68% different from the theoretical time of 20.4 min. Figure 18 displays the normalized concentration curves for both the model and the experiment.

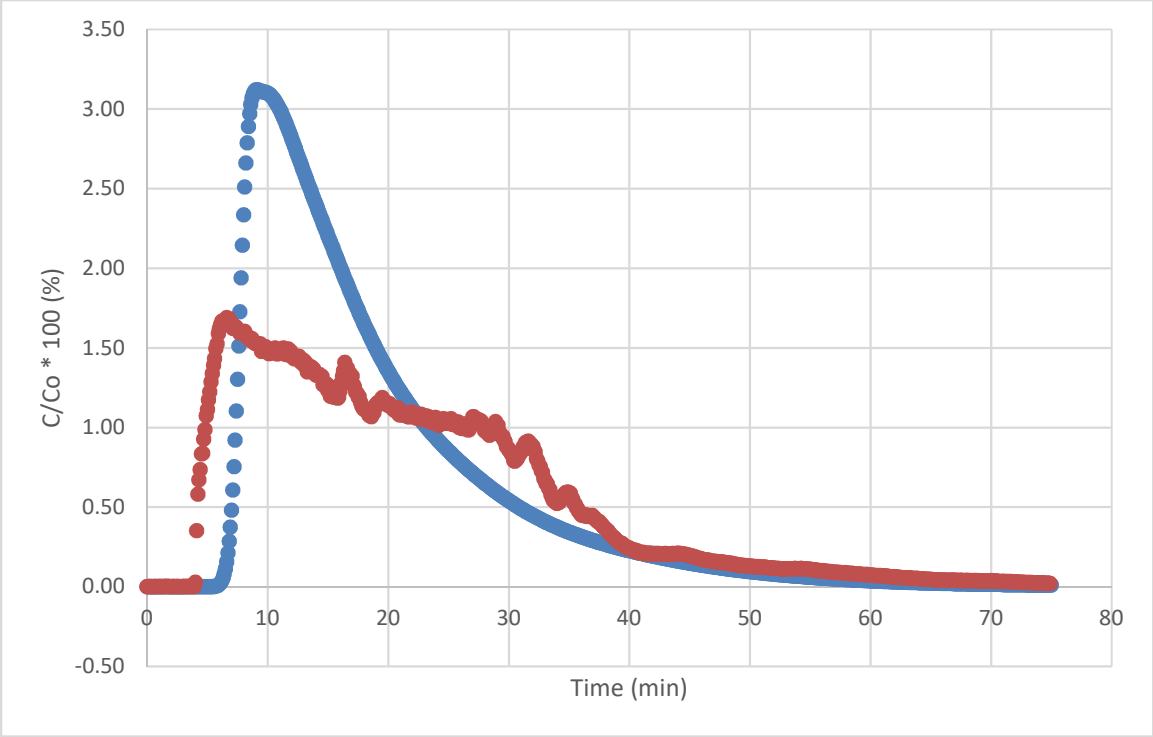

Figure 18. 2 mL/min Model and Experimental Concentration

Again, the curves have both similarities and differences. The qualitative peak difference is evident, but the degradation curve is more dissimilar at this flow rate than at 1 mL/min. The model peak is at 3.09% at 9.6 min, and the experiment peak is at 1.69% at 6.6 min. The model approaches zero at approximately 68.8 min, and the experiment at 74.9 min. The residence times, however, are within 11.44% of each other, with the model at 19.04 min and the experiment at 21.5 min.

4 mL/min Modeling Results, Analysis, and Comparison

The flow rate continues to increase, as the overall durations decrease. Figure 19 and 20 provide the multislice and streamline velocity plots from Study 1.

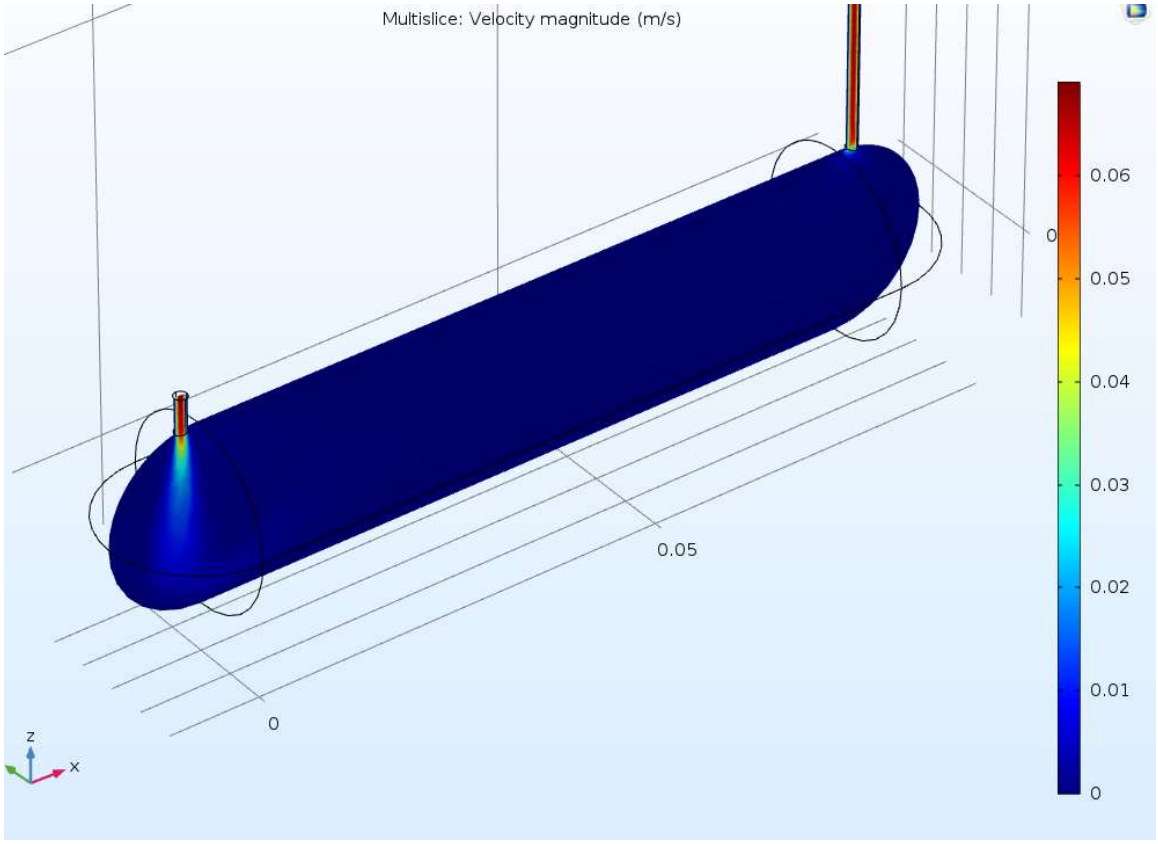

Figure 19. 4 mL/min Velocity Magnitude (m/s) Multislice

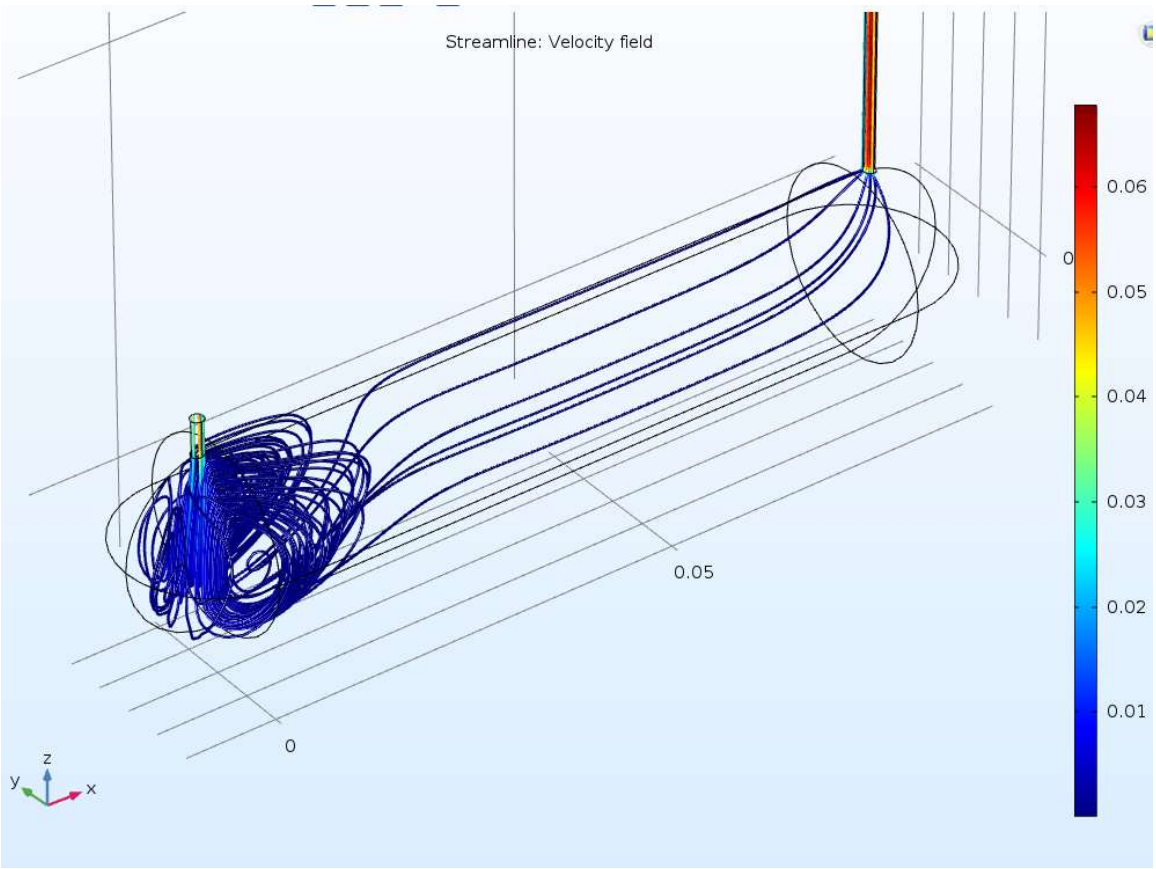

Figure 20. 4 mL/min Velocity Magnitude (m/s) Streamline

The velocity increases are evident in the plots as the scale increases in magnitude while the higher velocity liquid spreads further into the reactor body from the inlet. Additionally, the streamlines show more mixing than previously at the inlet. Figure 21 begins the results from Study 2 with the dye concentration passing through the reactor at .2 min and 4.5 min.

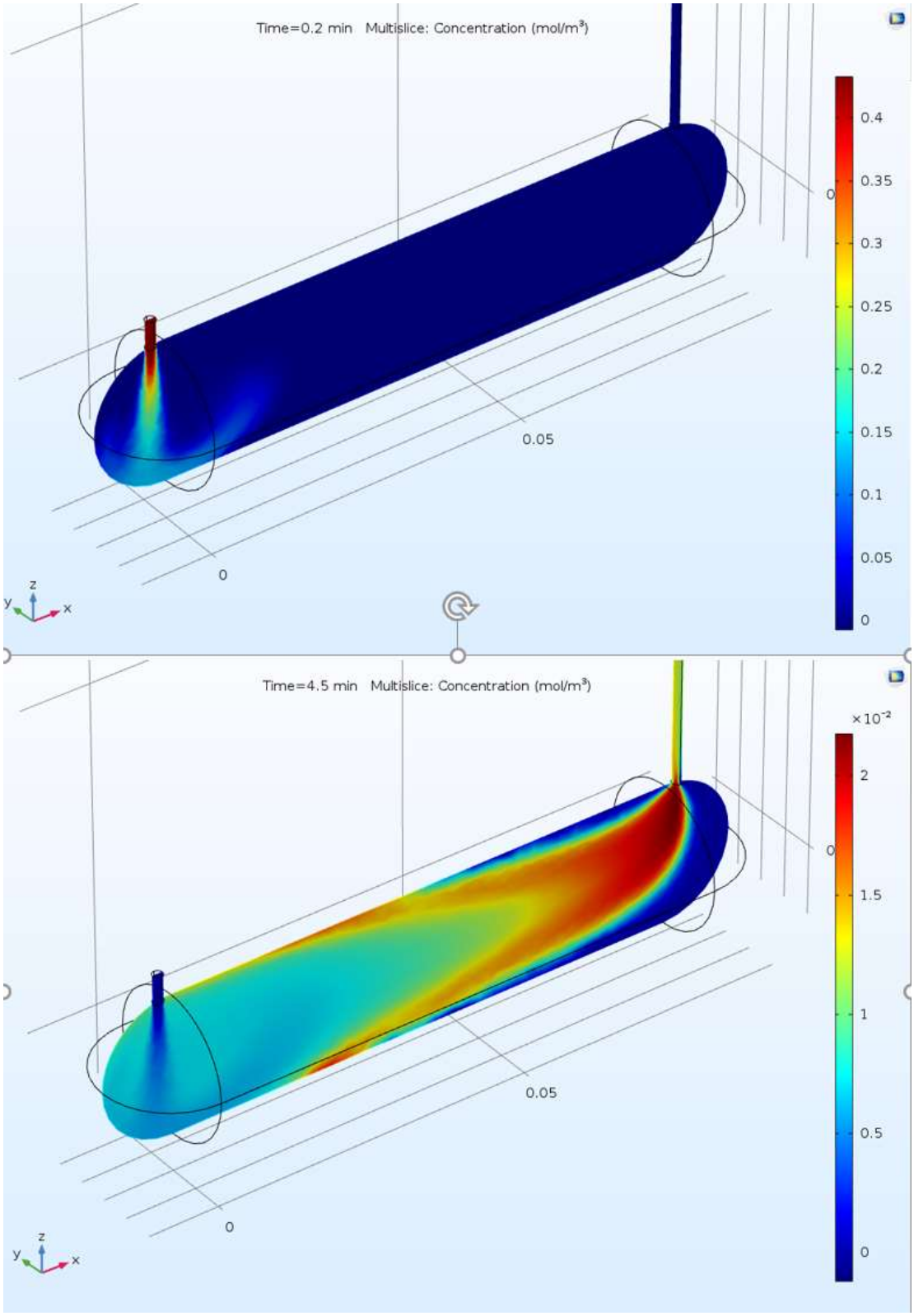

Figure 21. 4 mL/min Multislice Concentration at .2 min and 4.5 min

The final model output, the effluent concentration, is shown below in Figure 22.

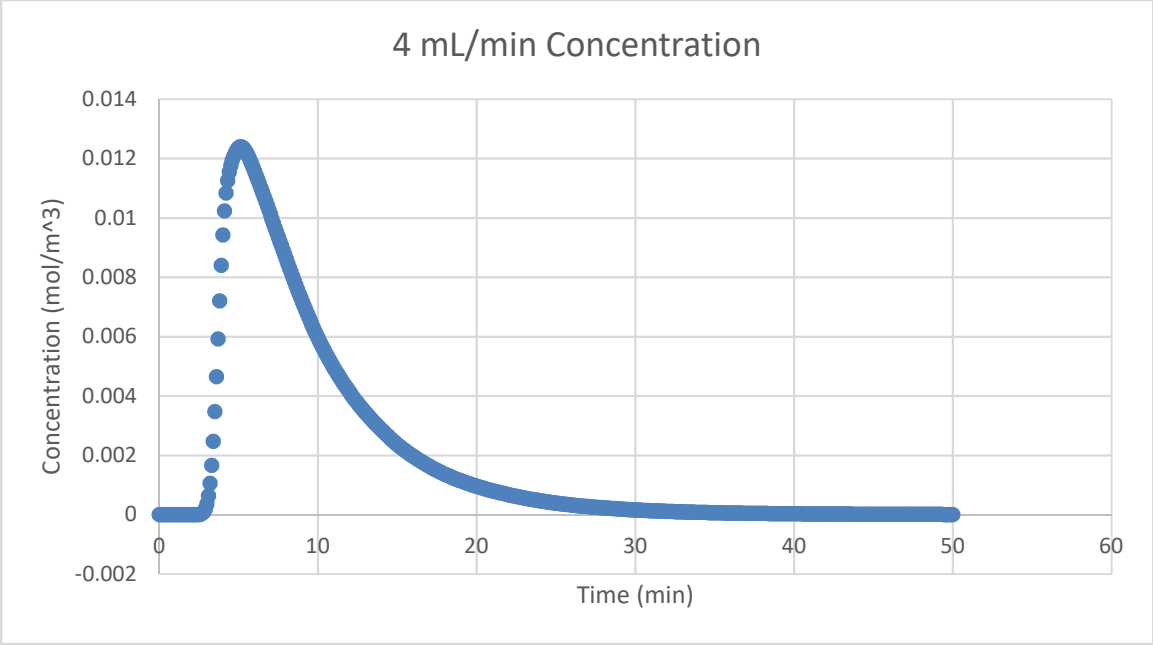

Figure 22. 4 mL/min Concentration

At this flow rate, the concentration has a similar concentration peak to 2 mL/min at 0.0122 mol/m^3 at 5.2 min, but approaches zero sooner at approximately 34.4 min. The residence time becomes 9.63 min, which is 5.62% different than the theoretical time of 10.2 min. Figure 23 compares the normalized model concentration curve to the normalized experimental curve.

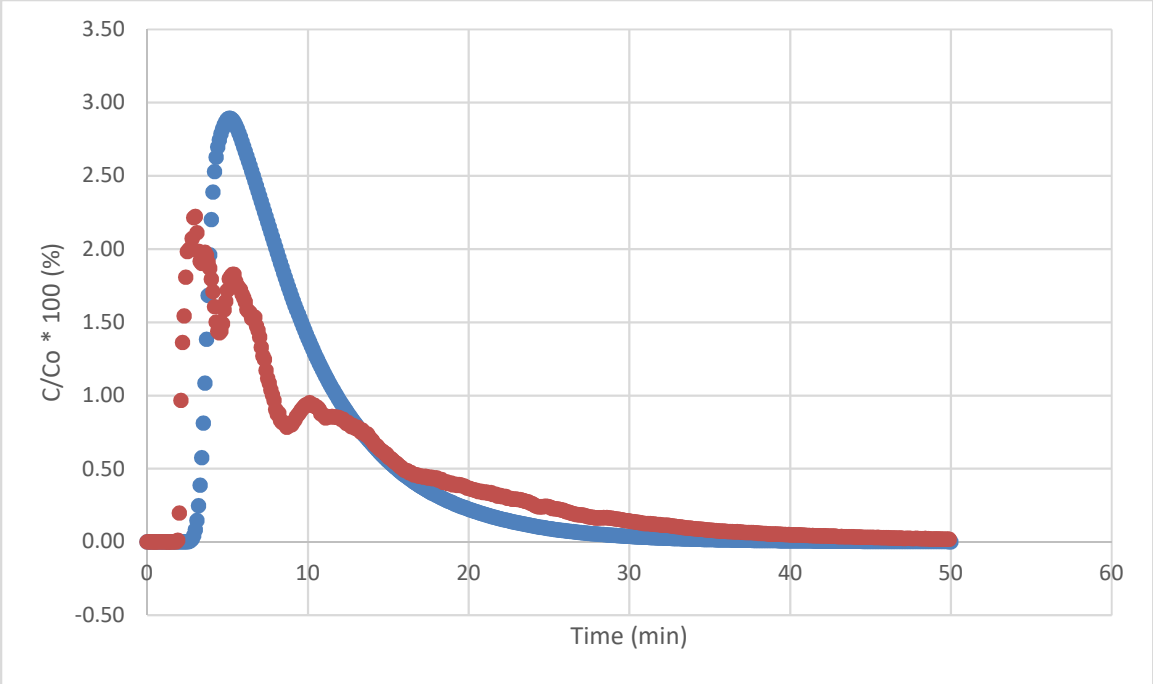

Figure 23. 4 mL/min Model and Experimental Concentration

At this flow rate, the qualitative comparison becomes more readily apparent. The peaks are still dissimilar, but they are closer than the lower flow rates, and the degradation curves appear to be more similar. Quantitatively, the model peaks at 2.85% at 5.2 min, and the experiment reaches 2.22% at 3 min. Although they may appear similar, further quantitative comparison reveals greater differences than expected. The model approaches zero at 34.4 min, with the experiment not until 49.9 min, a difference of over 15 min. In addition, the residence times are 18.8% different at 9.63 for the model and 11.86 for the experiment.

8 mL/min Modeling Results, Analysis, and Comparison

Finally, the 8 mL/min flow rate results are reported, beginning again with the velocity output from Study 1. Figure 24 shows the cross-sectional multislice velocity magnitude, and Figure 25 shows the streamlines.

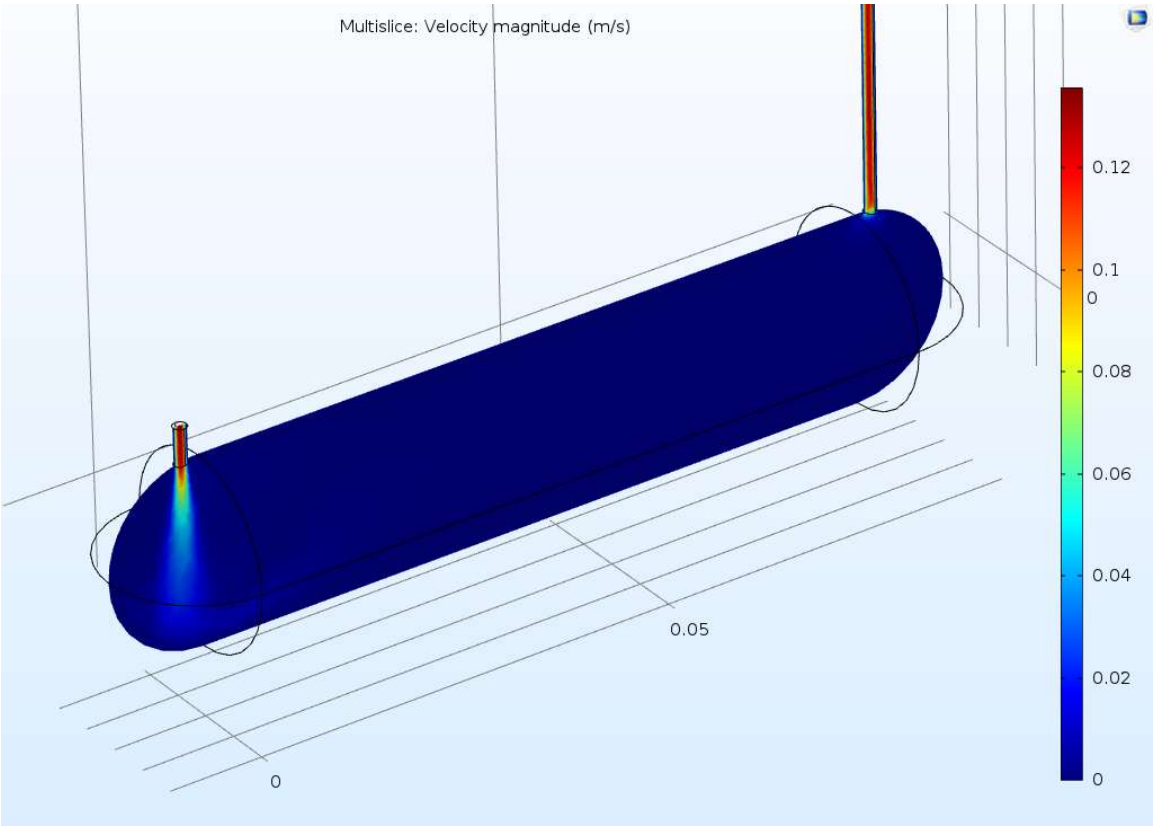

Figure 24. 8 mL/min Velocity Magnitude (m/s) Multislice

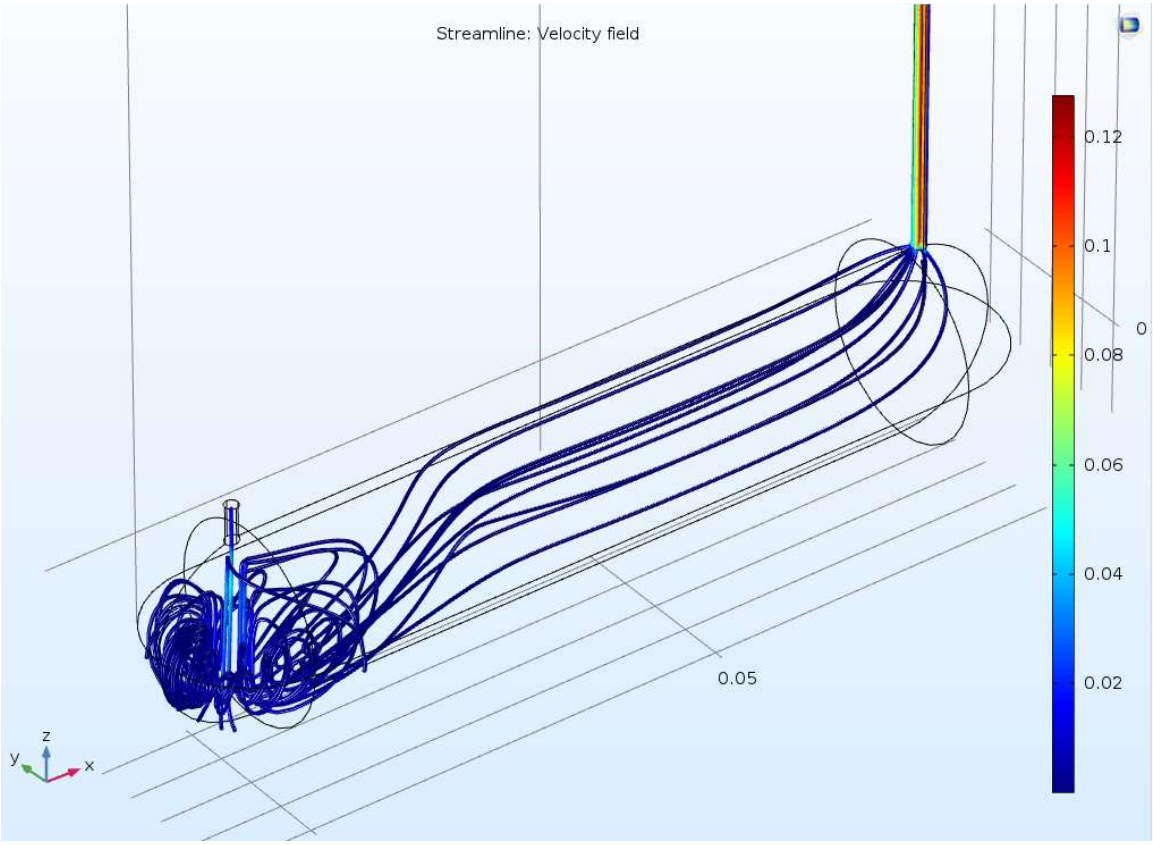

Figure 25. 8 mL/min Velocity Magnitude (m/s) Streamline

At this accelerated flow rate, it is clear in both charts that the reactor is experiencing higher velocities, not just at the inlet and outlet but further into the reactor body. The streamline chart shows the most mixing of all flow rates. The results from Study 2 are show below in Figure 26.

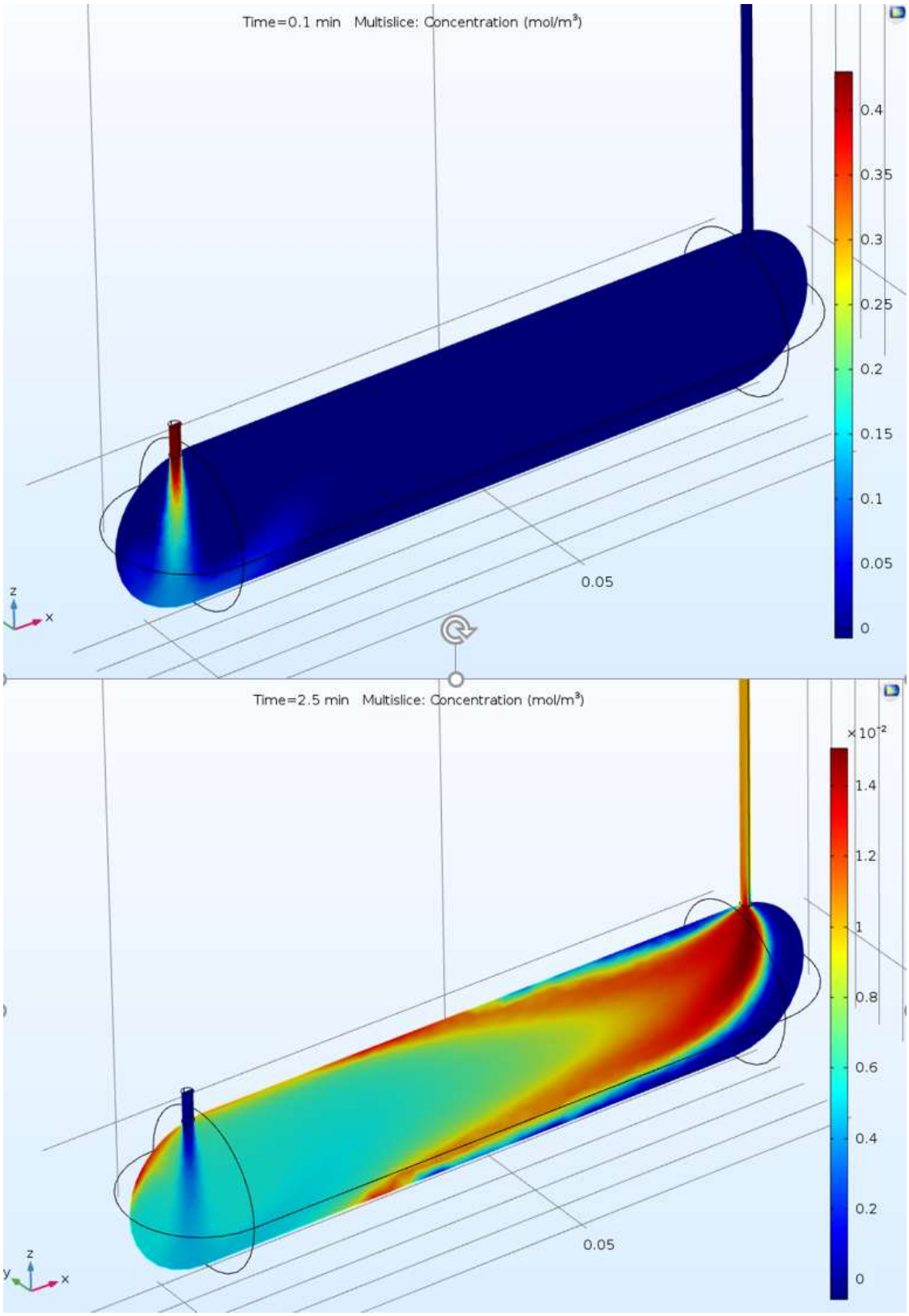

Figure 26. 8 mL/min Multislice Concentration at .1 min and 2.5 min

A trend of decreasing time iterations in the cross-sectional multislice concentration plots emerges as all the flow rates are reviewed. It is clear the concentration of dye is moving through the reactor more quickly each time as flow rate increases. The final model concentration output for 8 mL/min is Figure 27.

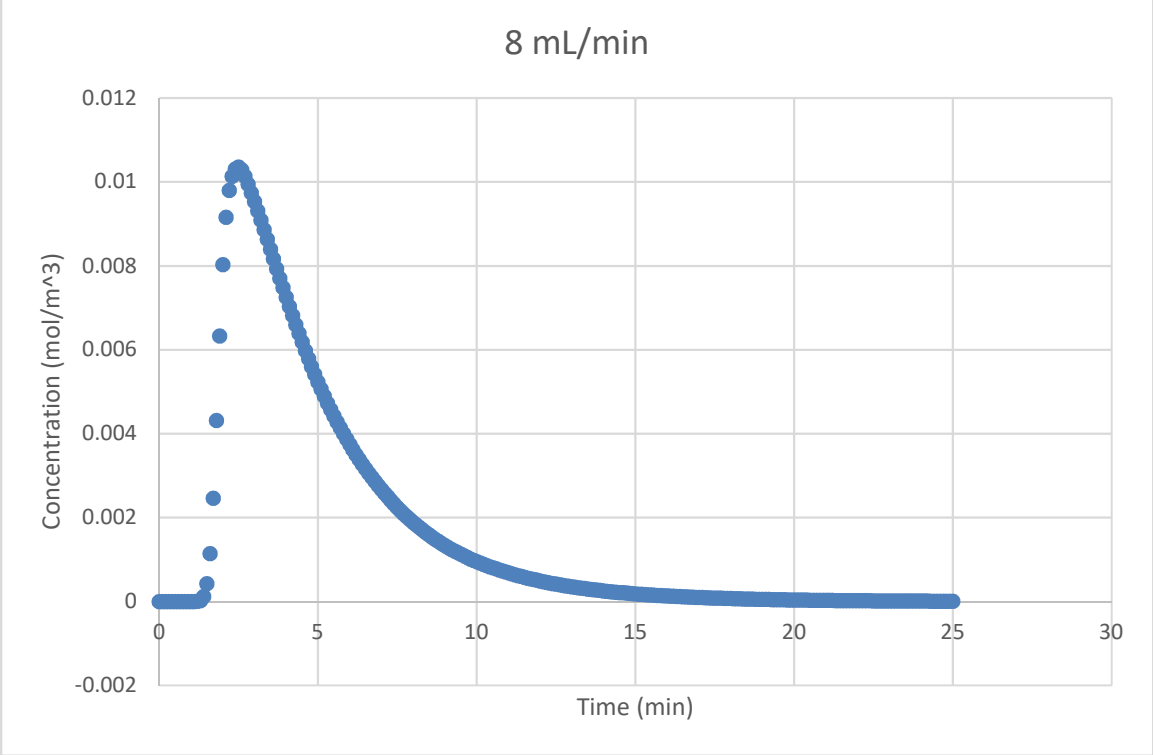

Figure 27. 8 mL/min Concentration

This flow rate produces the lowest concentration peak and earliest arrival at zero concentration of all the models. The peak is 0.0102 mol/m^3 at 2.39 min at zero concentration is at approximately 17.7 min. The residence time is 4.91 min, which is within 0.59% of the theoretical time of 5.1 min. In terms of residence time, the 8 mL/min model produces the most accurate representation. Figure 28 below compares this model to the experimental results.

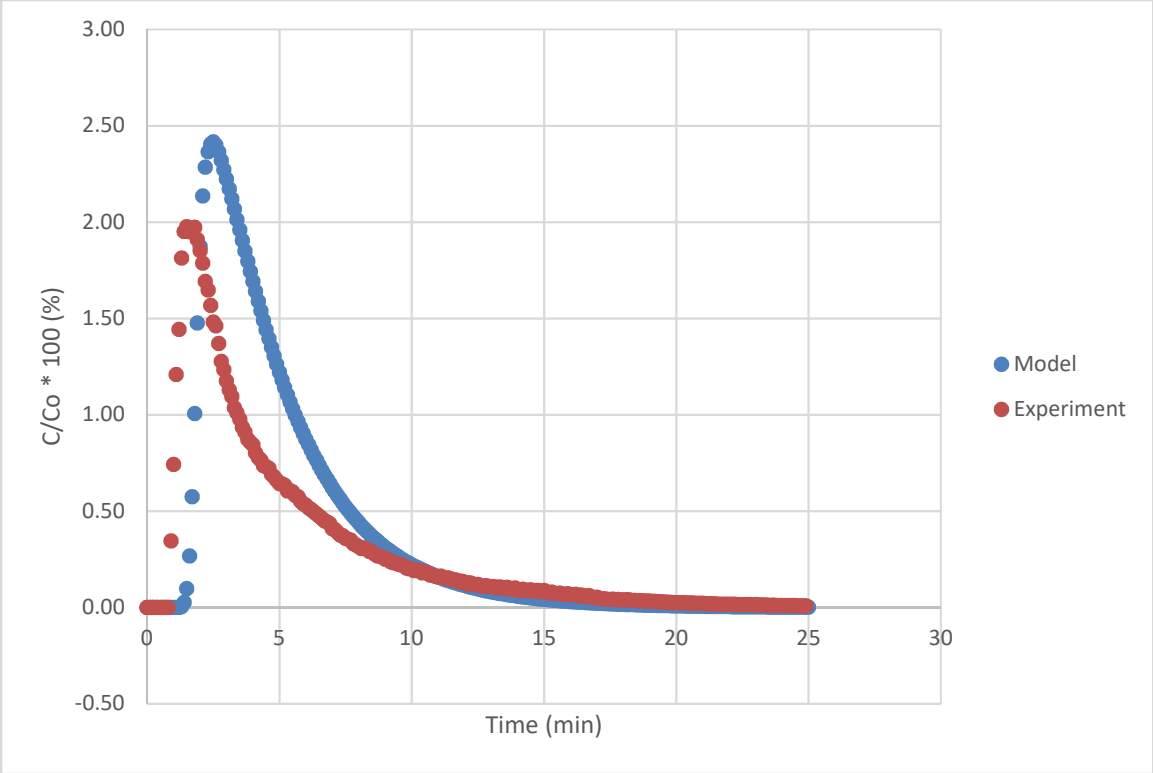

Figure 28. 8 mL/min Model and Experimental Concentration

With this comparison, it becomes readily apparent that the 8 mL/min model has produced the most qualitatively and quantitatively similar results to the experimental data. The model peaks at 2.39% at 2.6 min, while the experiment peaks at 1.98% at 1.5 min. The model approaches zero at approximately 17.7 min, with the experiment taking slightly longer at 22.3 min. The residence times are within 3.6% of each other. The quantitative comparison data is compiled below in Table 2.

Table 2. Concentration Quantitative Comparison

	1 mL/min				
	Peak (%)	Time (min)	Zero (min)	HRT vs Observed Difference (%)	Experiment vs Model Difference (%)
Experiment	2.04	9.2	124.2	14.08	10.41
Model	4.6	19.6	148.8	5.11	

	2 mL/min				
	Peak (%)	Time (min)	Zero (min)	HRT vs Observed Difference (%)	Experiment vs Model Difference (%)
Experiment	1.69	6.6	74.9	5.14	11.44
Model	3.09	9.6	68.8	6.68	

	4 mL/min				
	Peak (%)	Time (min)	Zero (min)	HRT vs Observed Difference (%)	Experiment vs Model Difference (%)
Experiment	2.22	3	49.9	13.98	18.8
Model	2.85	5.2	34.4	5.62	

	8 mL/min				
	Peak (%)	Time (min)	Zero (min)	HRT vs Observed Difference (%)	Experiment vs Model Difference (%)
Experiment	1.98	1.5	22.3	0.59	3.6
Model	2.39	2.6	17.7	3.66	

It is also useful to directly compare the concentration curves between flow rates, similar to the experimental data, as shown in Figure 29.

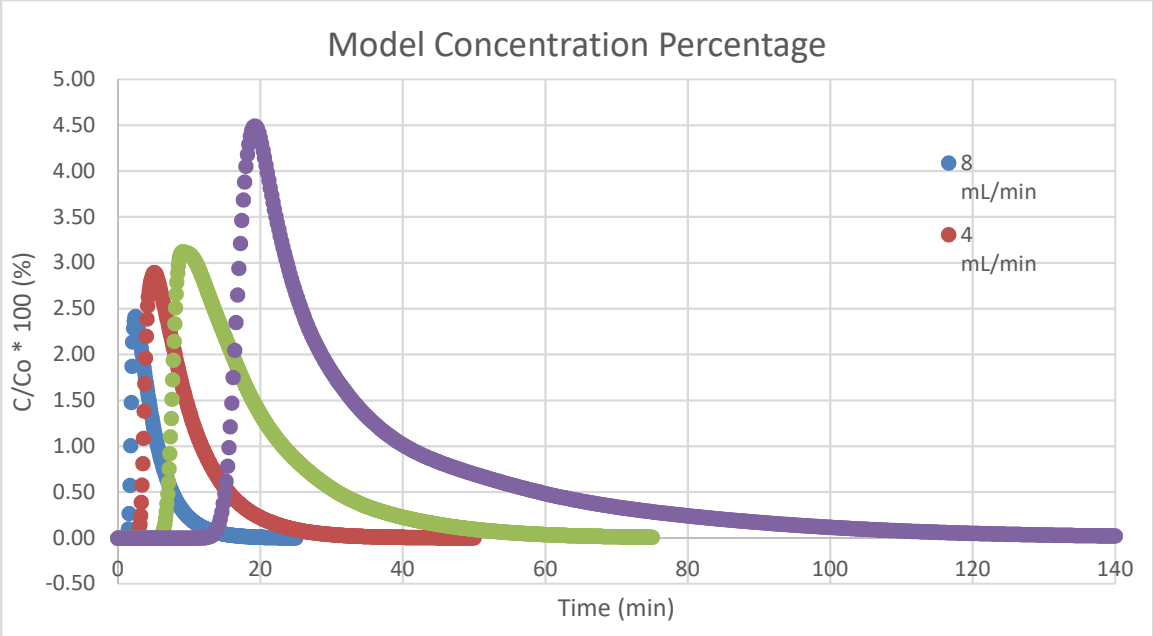

Figure 29. Model Concentration Percentage Comparison

This comparison clearly shows the effect of mixing on the concentration output. The peak concentration is lower at each subsequent flow rate as the dye has less time in the reactor to diffuse and experiences more convection and mixing, spreading the dye throughout the reactor.

Dispersion Comparison

The final characteristic used to gauge model effectiveness is the dispersion coefficient, or D value. As described in Chapter 2, the D value was calculated by minimizing the sum of squared error between a theoretical density curve and both the model and experimental concentration curves. Additionally, accounting for some dead zones in the reactor volume produced better fitting density curves and therefore more accurate D values, so each HRT has been reduced by a different factor to best match the experimental curve. The same factor was then applied to the HRT for the model curve. The curves are displayed below, grouped by flow rate with the model and experimental curves paired together, beginning with 1 mL/min in Figure 30 below.

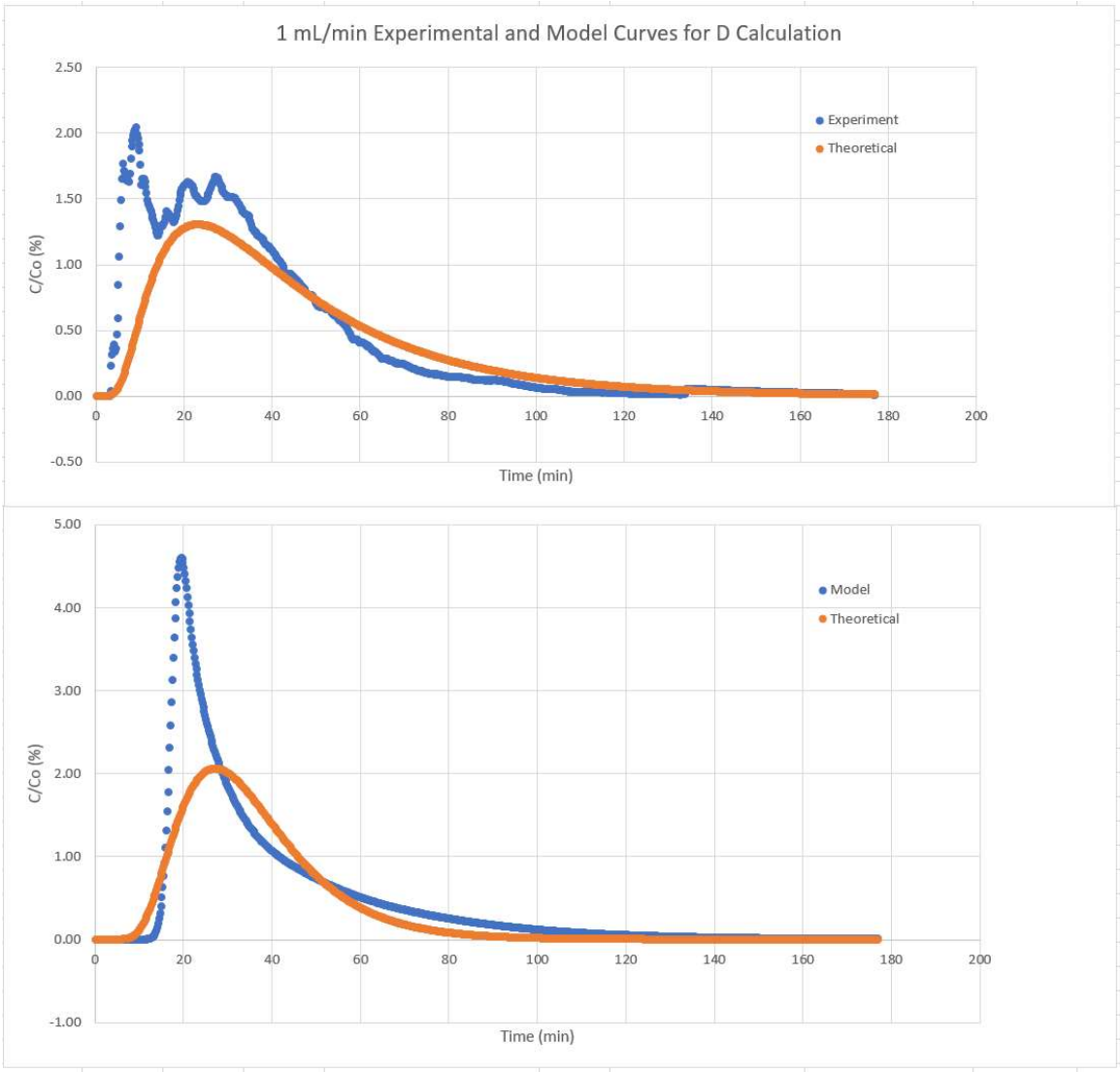

Figure 30. 1 mL/min Experimental and Model Curves for D Calculation

The D value calculated for the experimental data was 0.257, with an SSE of 74.28. The model produced a D value of 0.095 with an SSE of 204.2. The HRT was reduced by 26.5% from 40.8 min to 30 min. As a trend, it will become clear that the experimental data more closely fits the theoretical curve, yielding consistently lower SSE amounts than the model curves. Figure 31 below displays the 2 mL/min curves.

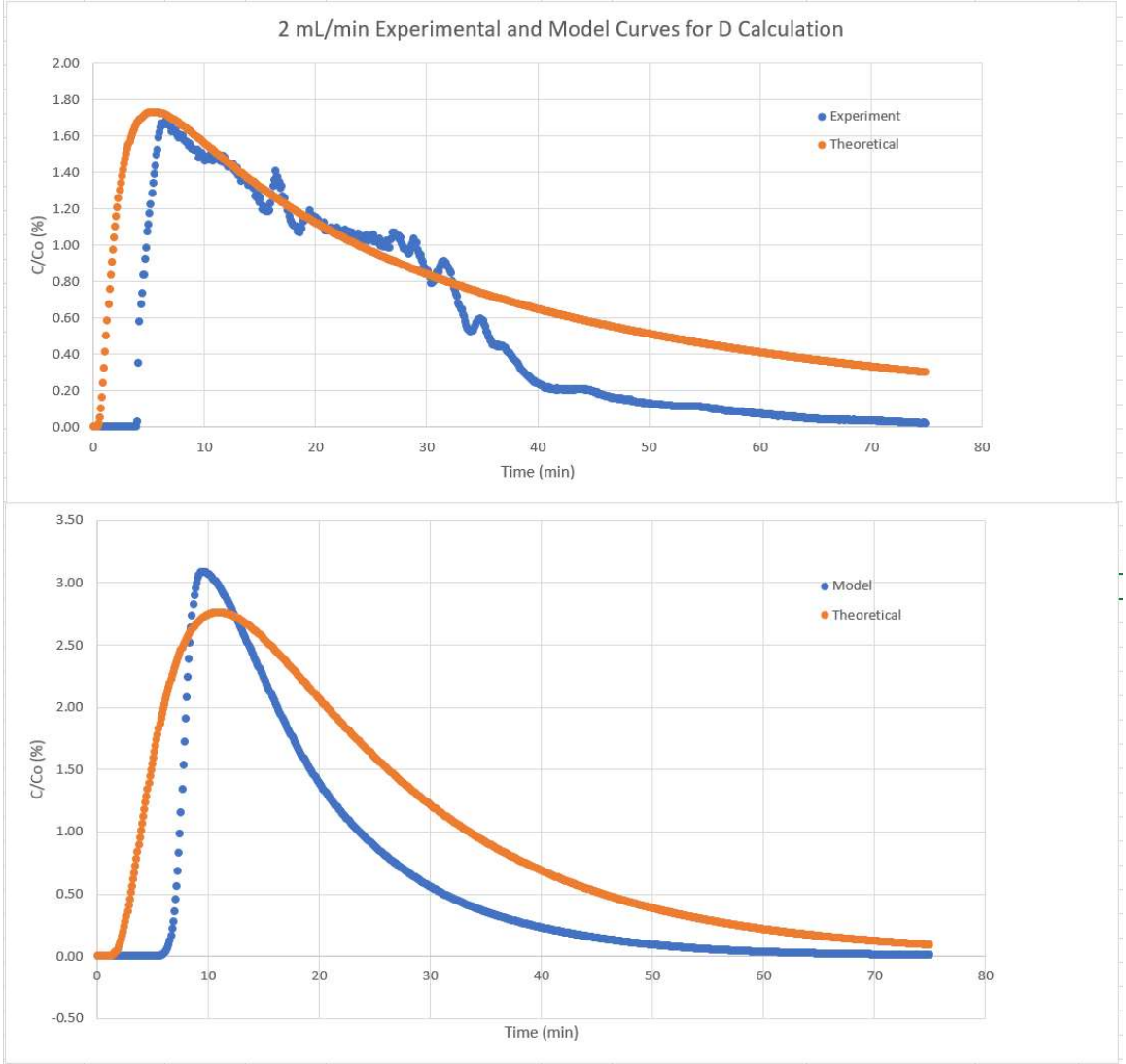

Figure 31. 2 mL/min Experimental and Model Curves for D Calculation

For the 2 mL/min experimental curve, the D value was 1.18 and the SSE was 109.85. The model produced a D value of 0.317 with an SSE of 238.4. The reduction factor was 26.47%, moving the HRT from 20.4 min to 15 min. Figure 32 below shows the curves for 4 mL/min.

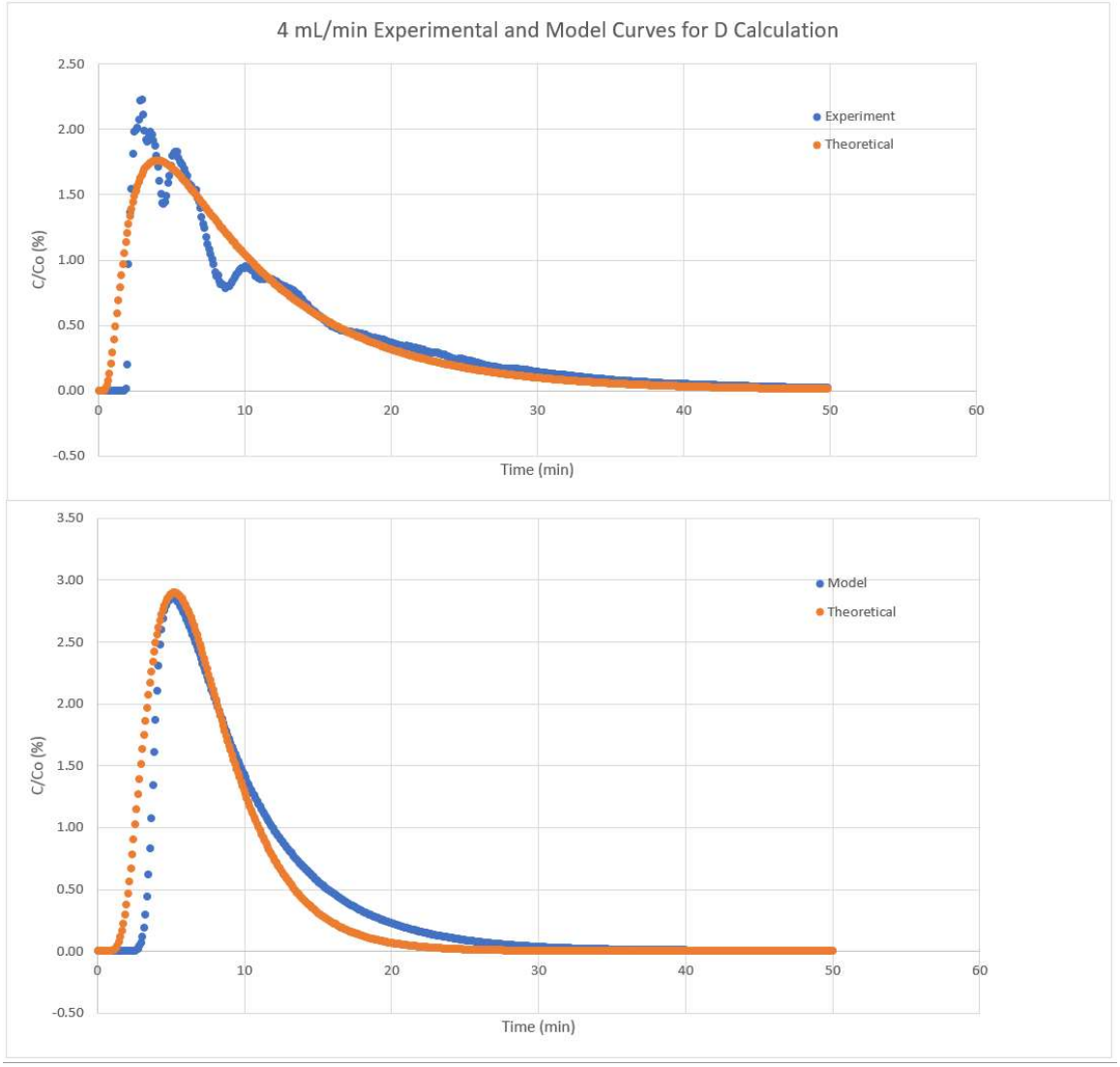

Figure 32. 4 mL/min Experimental and Model Curves for D Calculation

At this flow rate the experiment produced a D value of 0.402 with an SSE of 13.6, the lowest of all the curves. The model's D value was 0.130 with an SSE of 33.75. However, the reduction factor was the highest out of all the flow rates at 41.18%, reducing the HRT from 10.2 min to 6 min. Finally, the 8 mL/min curves are located below in Figure 33.

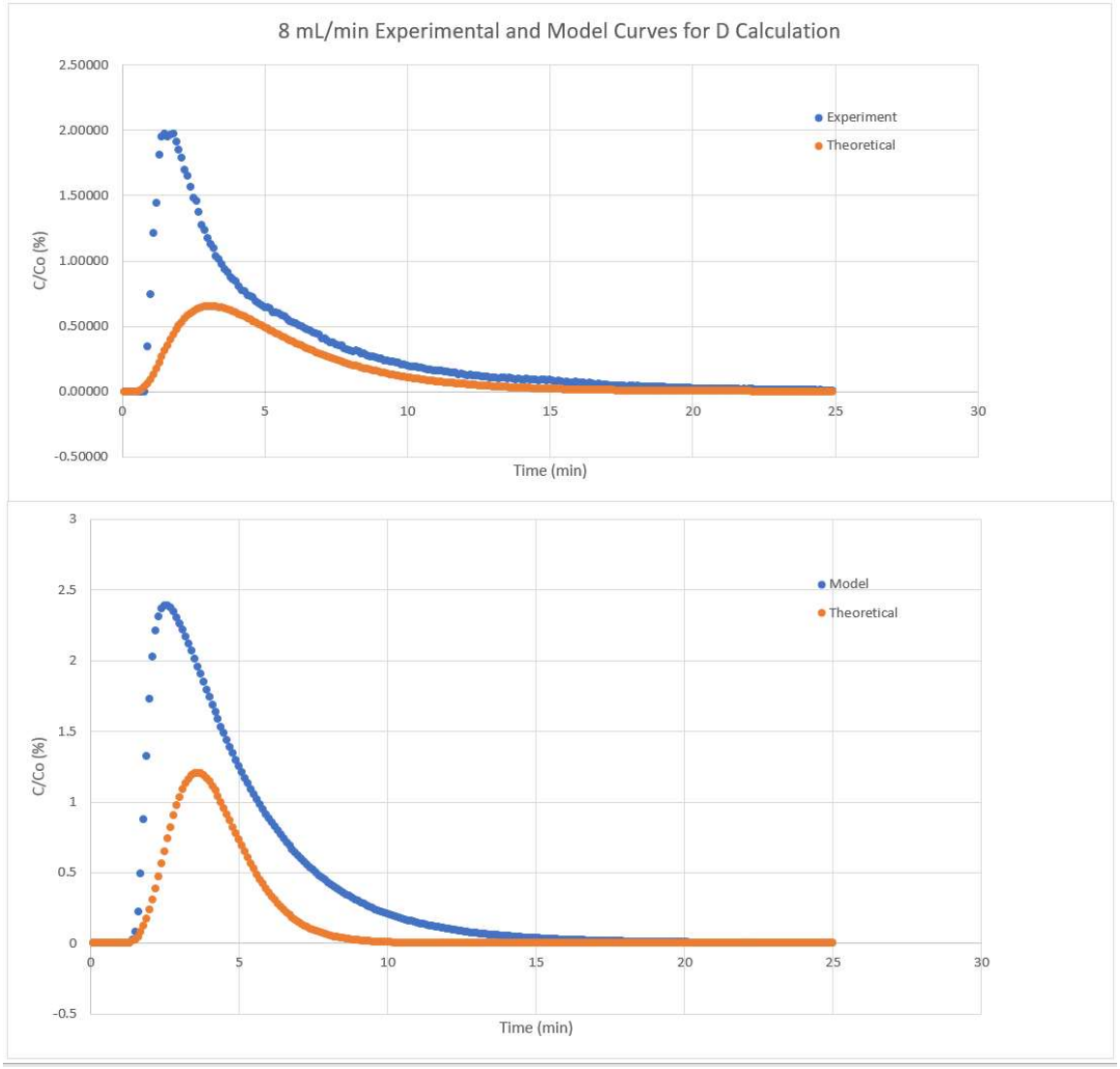

Figure 33. 8 mL/min Experimental and Model Curves for D Calculation

The 8 mL/min experiment produced a D value of 0.20 with an SSE of 33.3. The model produced a D value of 0.055 with an SSE of 49.75. The reduction was 25.5%, moving the HRT from 5.1 min to 3.8 min. Table 3 below summarizes the results.

Table 3. Dispersion Summary

	HRT	% Reduction	New HRT	Model D	Experimental D	% Difference	Model SSE	Experimental SSE
1 mL/min	40.8	26.47	30	0.0953	0.2572	62.9	204.22	74.28
2 mL/min	20.4	26.47	15	0.3171	1.1837	73.2	238.4	109.85
4 mL/min	10.2	41.18	6	0.1297	0.4021	67.7	33.75	13.6
8 mL/min	5.1	25.49	3.8	0.0548	0.2008	72.7	49.75	33.3

It becomes clear that the plug flow dispersion model fits the two higher flow rate curves significantly better than the two lower flow rate curves for both the experimental and model data. Additionally, the experimental data curves yield a better fit across all flow rates when compared to the model. Unfortunately, the differences in D coefficients between the model and experiment iterations are quite high. Even at 4 mL/min and 8 mL/min, where the theoretical curve fits the produced curve quite well, the differences in D values are 67.7% and 72.7% respectively. This supports the earlier conclusion that the model portrays transport by convection more accurately than it does the effects of diffusion.

Summary

The data reveals that while the experimental data is somewhat erratic at lower flow rates, the results become more predictable and more accurate as flow rates increase with regards to concentration. This could be due to the higher flow rates causing increased mixing experienced by the dye. Additionally, the model followed a similar trend of accuracy in terms of residence time as flow rates increased. The model's degradation curves portray ideal conditions that can be difficult to replicate in the laboratory, especially at lower flow rates where user error can have a larger influence. Furthermore, a comparison of the dispersion coefficients between the model and experiment prove to be less useful, as the model struggles to accurately recreate diffusion conditions. In all, the model proves its worth by accurately predicting the reactor HRT, which governs the critical contact time parameter for reactor efficiency.

V. Conclusion and Recommendations

This research analyzed a model's effectiveness to portray the fluid flow and species transport elements of a continuous flow UV LED water purification reactor. The model output concentration results were compared with laboratory experiment concentration results from the same reactor. Additionally, the velocity profile and concentration flow patterns were used to characterize the interaction occurring in the reactor. Finally, the concentration curves were used the calculate then compare dispersion coefficient between the model and experiment. The findings in this research may prove useful to the development of more complex models and eventually more efficient reactor prototypes.

Conclusions of Research

The degree of uncertainty with regards to the physical interactions between substances within the reactor becomes clear with this research. The model and experimental data overall produced similar residence times, meaning each molecule of dye was taking similar amounts of time to pass through the real and model reactor, but the manner at which they moved varied, especially at lower flow rates. It was not until the inflow reached 8 mL/min that the degradation curves and HRT for the model and the experimental data matched both qualitatively and quantitatively. The mixing effects of the higher flow rate contributed to a more even distribution of dye throughout the reactor and produced a more constant curve in the experimental data. At lower flow rates with less mixing and more diffusion, the model did not replicate the conditions in the reactor as accurately, although the percentage difference in residence times at between the model

and experiment at 1 mL/min was 10.4%, second only to the 8 mL/min flow rate. This may indicate the model reproduces the convection effect more accurately than the diffusion effect. Furthermore, supporting the previous conclusion, the model struggled to accurately recreate the dispersion coefficient produced by the experimental data. The 4 mL/min and 8 mL/min concentration curves from both the model and experiment matched the theoretical curve well, but the subsequent D value differed greatly. The model does seem to lack the refinement necessary to duplicate the complex diffusion and dispersion in the reactor.

Investigative Questions Answered

This research sought to answer three research questions. The first asked if a model can be created that accurately predicts the interaction between fluid flow and the transport of diluted species. The results indicate that in terms of residence times, interaction can be recreated with some degree of accuracy. The percentage difference between the theoretical and model residence times for the flow rates in order of increasing magnitude was 5.1%, 6.7%, 5.6%, and 0.6%. The accuracy was clearly higher at the 8 mL/min flow rate, most likely due to the convective mixing occurring in the reactor. However, both qualitatively and in terms of peak concentration percentage, the model did not recreate some of the concentration variation visible in the experimental data at lower flow rates. This may be a result of the model's difficulty reproducing the diffusion effect, or it may be from error introduced by the dye insertion technique.

The second question asked if the model can account for the variance in behavior due to varying flow rates. Overall the model does recreate the basic elements of species

transport at different flow rates. As the flow rate increases, the concentration peak percentage decreases, the time at which the concentration reaches the peak decreases, and the overall time until the concentration approaches zero decreases. However, the model lacks the likely variation in concentration present, especially at lower flow rates.

Finally, the third question asks if the model can be validated with laboratory results. The concentration variance in the laboratory results decreased as the flow rate increased. At lower flow rates, any dye injection errors were magnified in the concentration output, and uneven diffusion caused significant variance in concentration. This makes it difficult to use the laboratory data to validate the model data at lower flow rates, especially when the model data is not producing the same variations. Residence times, however, were still relatively useful validations at 1 mL/min and 2 mL/min, as the differences between the model and the experiment were 10.4% and 11.4% respectively. The 4 mL/min flow rate suffered the greatest difference at 18.8%. However, at 8 mL/min the laboratory data did validate the model data in terms of both qualitative degradation curve comparison and residence times. This suggests, in combination with previous research outlined in Chapter 2, that the model increases in accuracy as flow rate increases, therefore increasing its usefulness.

Significance of Research

This research is an important first step in integrating modeling into the reactor development process. Understanding the effect flow rate and physical geometry has on effluent concentration is an important factor in reactor optimization. A minimum flow rate of 40 mL/min (filtering 1 L of water in 25 min) would be required for a practical UV

LED point-of-use water purification reactor, so the model inaccuracies at lower flow rates would not be a factor. The lowest flow rate accurately modeled in published research as reviewed in Chapter 2 was 109 mL/min, so the accurate modeling at 8 mL/min proven viable by this research is unstudied territory and indicates there is a high level of usefulness for modeling in this application. Optimization by modeling rather than by multiple physical prototypes is much more efficient in terms of time, cost, and effort.

Recommendations for Future Research

COMSOL Multiphysics® Modeling Software is a powerful platform that is well-suited for this application. The entire prototyping process for reactor variations can be modeled and optimized prior to fabrication and laboratory testing. Specifically, models with higher flow rates and different geometries should be created and validated. Additionally, other aspects of the UV LED reactor should be modeled, to include UV ray optics and microbial inactivation. This would expedite the research and development process for the USAF to meet its goals of a lightweight, portable, and efficient water purification device.

Bibliography

Bolton, J. R., & Cotton, C. A. (2008). *The Ultraviolet Disinfection Handbook*.

Bolton, J. R., Dussert, B., Bukhari, Z., Hargy, T. M., & Clancy, J. L. (1998). Inactivation of Cryptosporidium parvum by Medium-Pressure Ultraviolet Light in Finished Drinking Water. In *The AWWA Annual Conference*. Denver, Colorado: AWWA.

Bowker, C., Sain, A., Shatalov, M., & Ducoste, J. (2011). Microbial UV fluence-response assessment using a novel UV-LED collimated beam system. *Water Research*, *45*(5), 2011–2019. http://doi.org/10.1016/j.watres.2010.12.005

Camelbak. (2017). *Camelbak All Clear Bottle*. Retrieved from http://shop.camelbak.com/all-clear-bottle

CDC. (2012). Drinking Water. Centers for Disease Control and Prevention. Retrieved from http://www.cdc.gov/healthywater

CDC. (2014). A Guide to Drinking Water Treatment Technologies for Home Use. Centers for Disease Control and Prevention. Retrieved from http://www.cdc.gov/healthywater

Chatterley, C., & Linden, K. (2010). Demonstration and evaluation of germicidal UV-LEDs for point-of-use water disinfection. *Journal of Water and Health*, *8*(3), 479–486. http://doi.org/10.2166/wh.2010.124

Chen, J., Deng, B., & Kim, C. N. (2011). Computational fluid dynamics (CFD) modeling of UV disinfection in a closed-conduit reactor. *Chemical Engineering Science*, *66*(21), 4983–4990. http://doi.org/10.1016/j.ces.2011.06.043

Clarke, S. (2006). Ultraviolet Light Disinfection in the Use of Individual Water Purification Devices Technical Information Paper # 31-006-0211. *U.S Army Public Health Command*, 1–12. http://doi.org/TIP #31-006-0211 ULTRAVIOLET

Clarke, S. H. (2006). *Iodine Disinfection in the Use of Individual Water Purification Devices*.

COMSOL. (2016). COMSOL Multiphysics. Retrieved from http://www.comsol.com

Crawford, M. H., Banas, M. a, Ross, M. P., Ruby, D. S., Nelson, J. S., Boucher, R., & Allerman, A. a. (2005). Final LDRD Report : Ultraviolet Water Purification Systems for Rural Environments and Mobile Applications, (November), 1–37.

Cruz-Díaz, M. R., Rivero, E. P., Almazán-Ruiz, F. J., Torres-Mendoza, Á., & González, I. (2014). Design of a new FM01-LC reactor in parallel plate configuration using numerical simulation and experimental validation with residence time distribution (RTD). *Chemical Engineering and Processing: Process Intensification*,

85(November), 145–154. http://doi.org/10.1016/j.cep.2014.07.010

Downes, A., & Blunt, T. P. (1878). On the influence of light upon photoplasm. *Proceedings of the Royal Society of London*, *28*, 199–212.

Earnest, G. S., & Gressel, M. (2003). *Guidance for Filtration and Air-Cleaning Systems to Protect Building Environments from Airborne Chemical, Biological, Radiological Attacks*. *National Institute for Occupational Safety and Health*.

EPA. (1999). Wastewater Technology Fact Sheet Clorine Disinfection. U.S. Environmental Protection Agency.

Federal Acquisition Regulation (2016).

Hamamoto, A., Mori, M., Takahashi, A., Nakano, M., Wakikawa, N., Akutagawa, M., … Kinouchi, Y. (2007). New water disinfection system using UVA light-emitting diodes. *Journal of Applied Microbiology*, *103*(6), 2291–2298. http://doi.org/10.1111/j.1365-2672.2007.03464.x

Holonyak, N., & Bevacqua, S. F. (1962). Coherent (visible) light emission from Ga(As1-xPx) junctions. *Applied Physics Letters*, *1*(4), 82–83. http://doi.org/10.1063/1.1753706

Hydro-Photon. (2016). SteriPEN. Retrieved from http://www.steripen.com

James, S. (2017). *Investigating Point-of-Use UV-LED Water Purification Device using Computation Multiphysics Modeling Software*. Air Force Institute of Technology.

Jenny, R. M., Jasper, M. N., Simmons, O. D., Shatalov, M., & Ducoste, J. J. (2015). Heuristic optimization of a continuous flow point-of-use UV-LED disinfection reactor using computational fluid dynamics. *Water Research*, *83*, 310–318. http://doi.org/10.1016/j.watres.2015.06.031

Jenny, R. M., Simmons III, O. D., Shatalov, M., & Ducoste, J. J. (2014). Modeling a continuous flow ultraviolet Light Emitting Diode reactor using computational fluid dynamics. *Chemical Engineering Science*, *116*(0), 524–535. http://doi.org/http://dx.doi.org/10.1016/j.ces.2014.05.020

Kovac, J., Peternai, L., & Lengyel, O. (2003). Advanced light emitting diodes structures for optoelectronic applications. *Thin Solid Films*, *433*(1–2 SPEC.), 22–26. http://doi.org/10.1016/S0040-6090(03)00314-6

Kowalski, W. (2009). *Ultraviolet Germicidal Iradiation Handbook*. Berlin Heidelberg: Springer-Verlag.

Kozisek, F. (2005). *Nutrients in Drinking Water*.

Lawrence, B. J., Devarapalli, M., & Madihally, S. V. (2009). Flow dynamics in bioreactors containing tissue engineering scaffolds. *Biotechnology and Bioengineering*, *102*(3), 935–947. http://doi.org/10.1002/bit.22106

LED. (2016). In *Encyclopaedia Britannica*. Retrieved from http://www.britannica.com/technology/LED

Lenk, R., & Lenk, C. (2011). *Practical Lighting Design with LEDs*. Hoboken, NJ: John Wiley & Sons, Inc.

Levenspiel, O. (1999). *Chemical reaction engineering*. *Ind. Eng. Chem. Res* (Vol. 38). http://doi.org/10.1021/ie990488g

Meulemans, C. C. E. (1987). The Basic Principles of UV-Disinfection of Water. *Ozone: Science & Engineering*, *9*(4), 299–313.

Muramoto, Y., Kimura, M., & Nouda, S. (2015). Development and future of ultraviolet light-emitting diodes ~uV-LED will replace UV lamp~. *2015 IEEE Summer Topicals Meeting Series, SUM 2015*, 13–14. http://doi.org/10.1109/PHOSST.2015.7248169

Nakamura, S., Mukai, T., & Senoh, M. (1994). emitting diodes Candela-class high-brightness InGaN / AIGaN, 1687–1689. http://doi.org/10.1063/1.111832

Nobelprize.org. (2014). Niels Ryberg Finsen - Facts. Retrieved from http://www.nobelprize.org/nobel_prizes/medicine/laureates/1903/finsen-facts.html

Oguma, K., Kita, R., Sakai, H., Murakami, M., & Takizawa, S. (2013). Application of UV light emitting diodes to batch and flow-through water disinfection systems. *Desalination*, *328*, 24–30. http://doi.org/10.1016/j.desal.2013.08.014

Perkin, F. M. (1910). Mercury Vapor Lamps and Action of Ultra Violet Rays. London: Faraday Society.

Pirnie, M., Linden, K. G., & Malley, J. P. J. (2006). Ultraviolet disinfection guidance manual for the final long term 2 enhanced surface water treatment rule. *Environmental Protection*, *2*(11), 1–436.

Reed, N. G. (2010). The history of ultraviolet germicidal irradiation for air disinfection. *Public Health Reports*, *125*(1), 15–27. Retrieved from http://www.pubmedcentral.nih.gov/articlerender.fcgi?artid=2789813&tool=pmcentrez&rendertype=abstract%5Cnhttp://www.pubmedcentral.nih.gov/articlerender.fcgi?artid=2789813%7B&%7Dtool=pmcentrez%7B&%7Drendertype=abstract

Schneider Jr., W. (2009). *Buying Commercial : Gaining the Cost/Schedule Benefits for Defense Systems*. *Science*.

Schubert, E. F. (2006). *Light-Emitting Diodes*. *Cambridge Universtiy Press*. http://doi.org/http://dx.doi.org/10.1017/CBO9780511790546

Shur, M. S., & Gaska, R. (2008). III-nitride Based Deep Ultraviolet Light Sources. *Proceedings of SPIE*, *6894*(689419), 689418–689419. http://doi.org/DOI: 10.1117/12.769128

Spencer, M. (2014). *Design Considerations for a Water Treatment System Utilizing Ultra-Violet Light Emitting Diodes*. Air Force Institute of Technology.

USEPA. (1999). 25 Years of the Safe Drinking Water Act: History and Trends. U.S. Environmental Protection Agency.

Vilhunen, S., Särkkä, H., & Sillanpää, M. (2009). Ultraviolet light-emitting diodes in water disinfection. *Environmental Science and Pollution Research*, *16*(4), 439–442. http://doi.org/10.1007/s11356-009-0103-y

Wang, Z., Liu, J., Dai, Y., Dong, W., Zhang, S., & Chen, J. (2012). CFD modeling of a UV-LED photocatalytic odor abatement process in a continuous reactor. *Journal of Hazardous Materials*, *215–216*(February), 25–31. http://doi.org/10.1016/j.jhazmat.2012.02.021

Werts, M. H. V., Raimbault, V., Texier-Picard, R., Poizat, R., Français, O., Griscom, L., & Navarro, J. R. G. (2012). Quantitative full-colour transmitted light microscopy and dyes for concentration mapping and measurement of diffusion coefficients in microfluidic architectures. *Lab on a Chip*, *12*(4), 808. http://doi.org/10.1039/c2lc20889j

Wols, B. A., Hofman, J. a. M. H., Uijttewaal, W. S. J., Rietveld, L. C., & van Dijk, J. C. (2010). Evaluation of different disinfection calculation methods using CFD. *Environmental Modelling & Software*, *25*(4), 573–582. http://doi.org/10.1016/j.envsoft.2009.09.007

Appendix A.

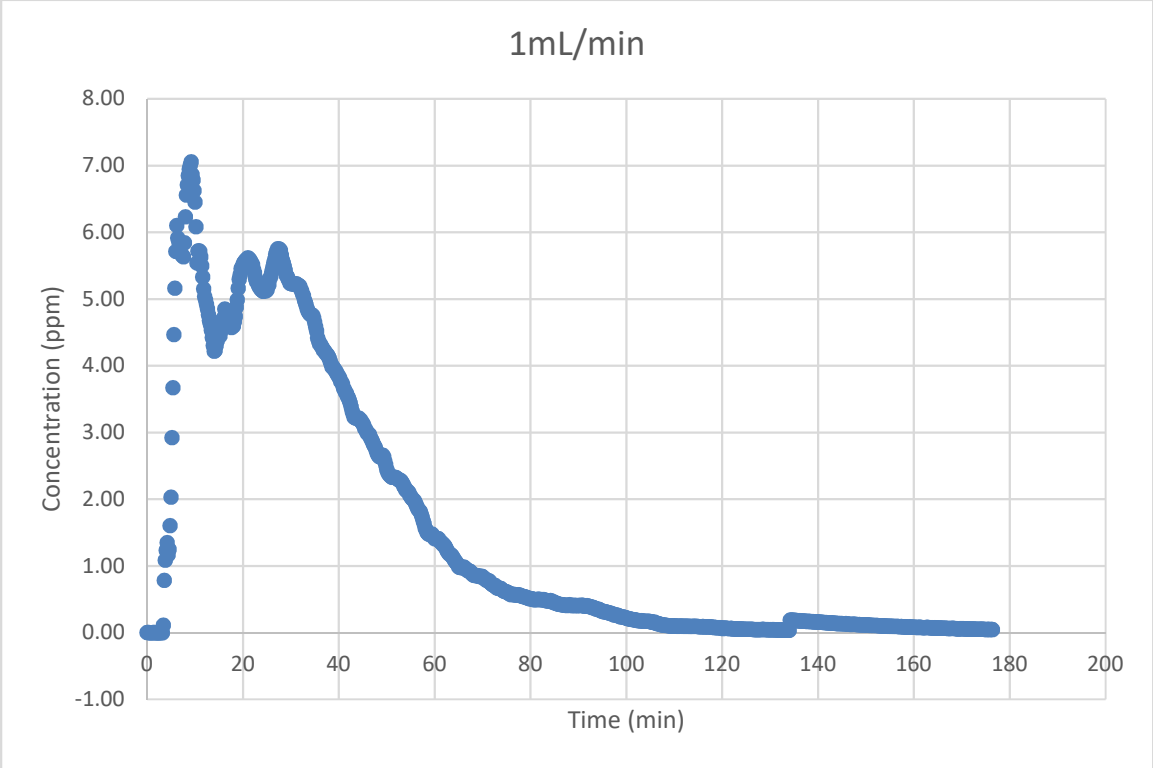

Figure 34. 1 mL/min Concentration

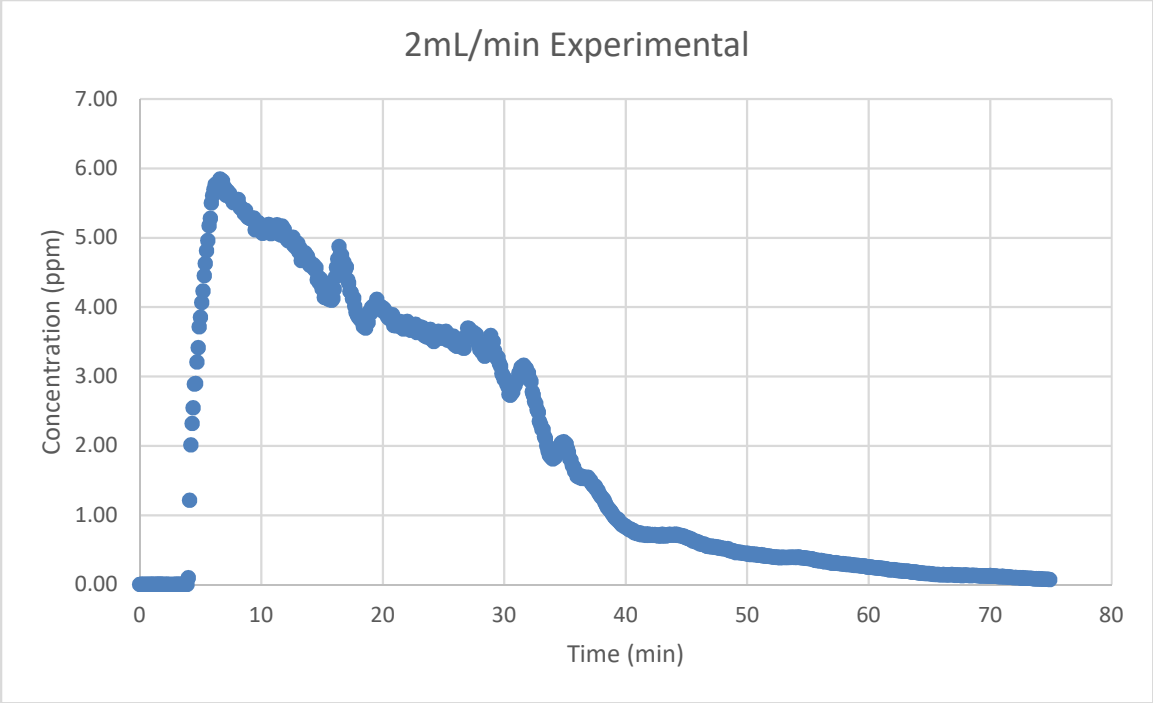

Figure 35. 2 mL/min Concentration

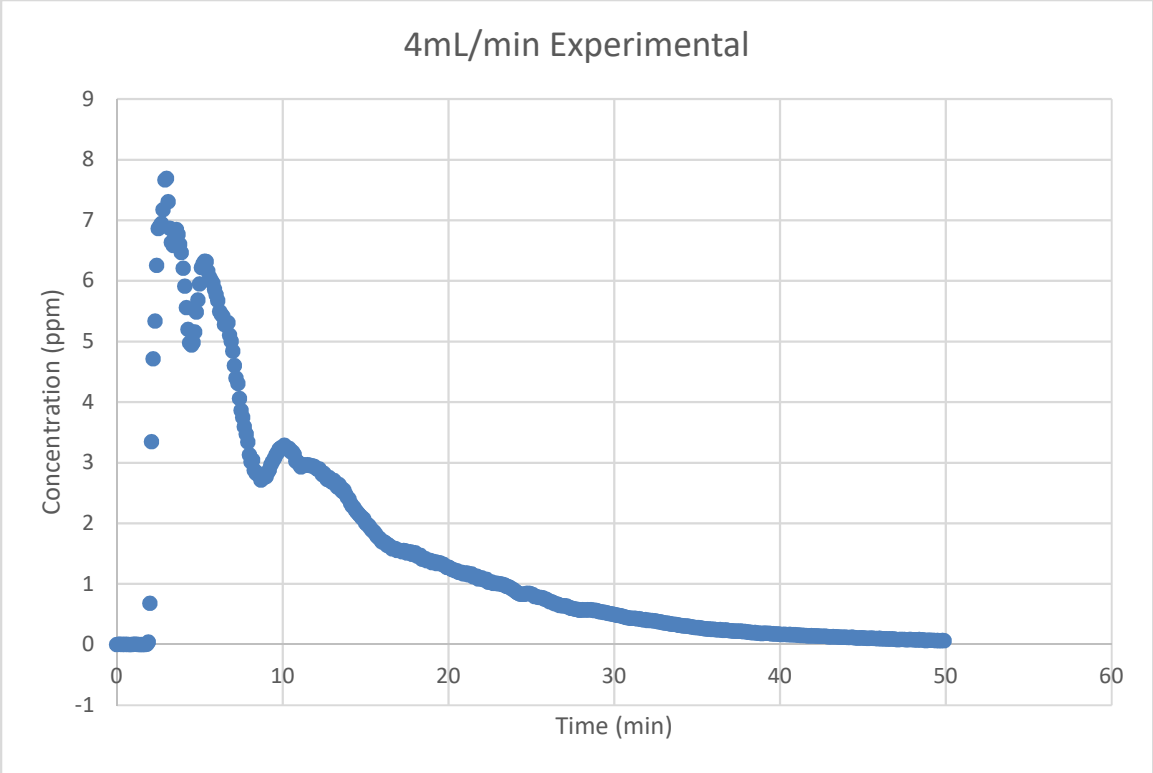

Figure 36. 4 mL/min Concentration

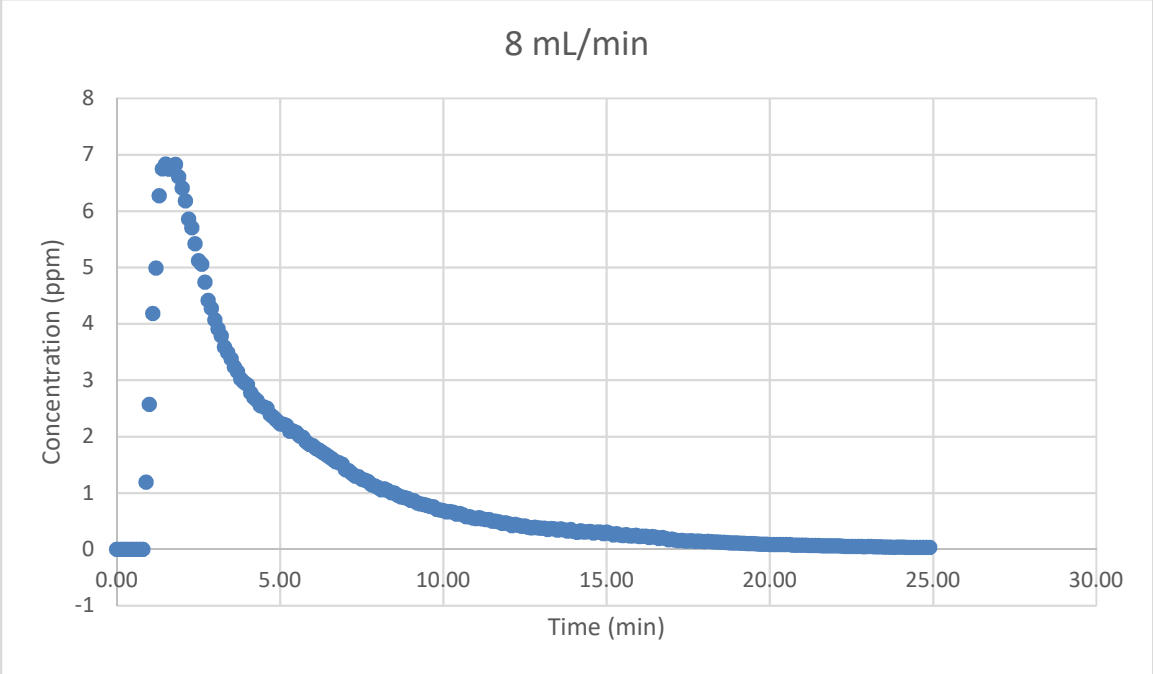

Figure 37. 8 mL/min Concentration

REPORT DOCUMENTATION PAGE

Form Approved
OMB No. 074-0188

PLEASE DO NOT RETURN YOUR FORM TO THE ABOVE ADDRESS.

1. REPORT DATE *(DD-MM-YYYY)*	2. REPORT TYPE	3. DATES COVERED *(From – To)*
03-03-2017	Master's Thesis	Sept 2015 – March 2017

TITLE AND SUBTITLE

Modeling and Validating a Continuous Flow Ultraviolet Light Emitting Diode Water Purification Reactor

5a. CONTRACT NUMBER

5b. GRANT NUMBER

5c. PROGRAM ELEMENT NUMBER

6. AUTHOR(S)

Kohlhepp, David A., Capt

5d. PROJECT NUMBER

5e. TASK NUMBER

5f. WORK UNIT NUMBER

7. PERFORMING ORGANIZATION NAMES(S) AND ADDRESS(S)
Air Force Institute of Technology
Graduate School of Engineering and Management (AFIT/ENY)
2950 Hobson Way, Building 640
WPAFB OH 45433-8865

8. PERFORMING ORGANIZATION REPORT NUMBER

AFIT-ENV-MS-17-M-198

9. SPONSORING/MONITORING AGENCY NAME(S) AND ADDRESS(ES)

US Environmental Protection Agency
25 W. Martin Luther King Dr.
Mailstop NG-16
Cincinnati, OH 45268
Matthew Magnuson, (513) 569-7321, magnuson.matthew@epa.gov

10. SPONSOR/MONITOR'S ACRONYM(S)

AFRL/RHIQ (example)

11. SPONSOR/MONITOR'S REPORT NUMBER(S)

12. DISTRIBUTION/AVAILABILITY STATEMENT
DISTRUBTION STATEMENT A. APPROVED FOR PUBLIC RELEASE; DISTRIBUTION UNLIMITED.

13. SUPPLEMENTARY NOTES
This material is declared a work of the U.S. Government and is not subject to copyright protection in the United States.

14. ABSTRACT

The Department of Defense has a need for a small, man-portable, point of use water purification device that is not currently available commercially in a configuration that meets all the use requirements. A device that utilizes ultraviolet (UV) light-emitting diodes (LEDs) to continuously treat water flowing from a "dirty" reservoir to a "clean" reservoir with low weight and power penalties would meet those requirements. This research pursued the development of such a device through the use of computer modeling, specifically in the area of computational fluid dynamics (CFD) and transport of diluted species. It sought to validate the use of the model for design optimization by duplicating concentration tracer tests accomplished in a laboratory with a prototype UV LED reactor at four different flow rates. By measuring the tracer concentration over time at the reactor effluent, the model results were compared to the experimental data qualitatively by the residence time density functions and quantitatively by hydraulic residence times, density curve characteristics, and the dispersion coefficient. The research found that the model has difficulty accurately reproducing the experimental results at lower flow rates, but finds success at the higher rates, rendering the model a useful tool for prototype design and development.

15. SUBJECT TERMS
Continuous Flow UV LED Water Purification Reactor Modeling

16. SECURITY CLASSIFICATION OF:			17. LIMITATION OF ABSTRACT	18. NUMBER OF PAGES	19a. NAME OF RESPONSIBLE PERSON
a. REPORT	b. ABSTRACT	c. THIS PAGE			Michael E. Miller, AFIT/ENV
U	U	U	UU	88	19b. TELEPHONE NUMBER *(Include area code)* (937) 255-3636, ext 4651 (michael.miller@afit.edu)

Standard Form 298 (Rev. 8-98)
Prescribed by ANSI Std. Z39-18